world weather attribution

Attribution of severe low rainfall in southern Madagascar, 2019-21

Authors

Luke J. Harrington[1], Piotr Wolski[2], Izidine Pinto[2,7], Anzela Mamiarisoa Ramarosandratana[3], Rondrotiana Barimalala[4], Robert Vautard[5], Sjoukje Philip[6], Sarah Kew[6], Roop Singh[7], Dorothy Heinrich[7], Julie Arrighi[7,8,9], Emmanuel Raju[10], Lisa Thalheimer[11], Thierry Razanakoto[12], Maarten van Aalst[7,8,13], Sihan Li[14], Remy Bonnet[5], Wenchang Yang[15], Friederike E. L. Otto[16], Geert Jan van Oldenborgh[6]

[1]New Zealand Climate Change Research Institute, Victoria University of Wellington, Wellington 6012, New Zealand

[2]Climate System Analysis Group, University of Cape Town, Cape Town, South Africa

[3]Direction des recherches et développement hydrométéorologiques" , Direction Générale de la Météorologie', Antananarivo, Madagascar

[4]Department of Oceanography University of Cape Town, Cape Town, South Africa

[5]Institut Pierre-Simon Laplace, CNRS, Sorbonne Université, Paris, France

[6]Royal Netherlands Meteorological Institute (KNMI), De Bilt, The Netherlands

[7]Red Cross Red Crescent Climate Centre, The Hague, the Netherlands

[8]Faculty of Geo-Information Science and Earth Observation (ITC), University of Twente, Enschede, the Netherlands

[9]Global Disaster Preparedness Center, American Red Cross, Washington DC, USA

[10]Global Health Section, University of Copenhagen, Copenhagen, Denmark

[11]Princeton University Woodrow Wilson School of Public and International Affairs: Princeton, NJ, US.

[12]Centre d'Etudes et de Recherches Economiques pour le Développement (CERED), Université d'Antananarivo, Madagascar

[13]International Research Institute for Climate and Society, Columbia University, New York, USA

[14]School of Geography and the Environment, University of Oxford, UK

[15]Department of Geosciences, Princeton University, Princeton, 08544, USA

[16]Grantham Institute, Imperial College London, UK

Main findings

- Southern Madagascar has been facing a severe food security crisis, made significantly worse by well below average rainfall from July 2019 to June 2021. This exceptional drought has

affected a region with high pre-existing levels of vulnerability to food insecurity, and the impacts have been compounded by COVID-19 restrictions and pest infestations.

- Madagascar is one of the poorest countries of the world, with a particularly high proportion of people living below the poverty line in the south of the country. This makes it difficult for local communities to cope with any prolonged period of drought, particularly when subsistence agriculture and pastoralism in the region is rain-fed only.

- We chose to analyse severe rainfall deficits in this study. This was because recent research found rainfall deficits were the primary driver of drought in regions of East Africa with very similar climatic properties to south-west Madagascar.

- The rainy seasons of both 2019/20 and 2020/21 saw just 60% of normal rainfall across the Grand Sud region. This lack of rain over the 24 months from July 2019 to June 2021 was estimated as a 1-in-135 year dry event, an event only surpassed in severity by the devastating drought of 1990-92.

- Large scale teleconnections did not significantly alter the likelihood of witnessing these exceptional rainfall deficits in southern Madagascar. While past episodes of anomalously low rainfall in the region have indeed coincided with moderate El Niño events, the severe El Niño of 1997/98 saw average levels of rain in the region, while the rainy season of 2020/21 was exceptionally dry despite coinciding with a moderate strength La Niña event.

- Based on observations and climate modeling, the occurrence of poor rains as observed from July 2019 to June 2021 in Southern Madagascar has not significantly increased due to human-caused climate change. While the observations and models combine to indicate a small shift toward more droughts like the 2019-2021 event as a consequence of climate change, these trends remain overwhelmed by natural variability.

- This result is consistent with previous research, with the IPCC's Sixth Assessment Report concluding that any perceptible changes in drought would only emerge in this region if global mean temperatures exceed 2°C above pre-industrial levels.

1. Introduction

Southern Madagascar is currently experiencing a food security crisis exacerbated by severe ongoing drought. In a region where 90% of the population is living below the poverty line, recent analyses by the Integrated Food Security Phase Classification group (IPC) have concluded that tens of thousands are currently facing severe famine-like conditions, which have worsened with consecutive rainy season failures in the otherwise semi-arid region.

In one of the hardest-hit districts of the Grand Sud (Grand South) region in Madagascar, Androy, half of all annual rainfall usually arrives during the peak months of the rainy season, from December to February, while only 20% of annual rainfall occurs during the six months from April to September (see Figure 1). However, for two consecutive rainy seasons in 2019/20 and 2020/21, only 60% of normal rain fell across the region, causing significant crop failures in a region of largely rain-fed subsistence agriculture and pastoralism. Similar back-to-back failures of the rainy season have

previously occurred in 2008-10 and 1990-92, with similar humanitarian impacts emerging then too (Benson & Clay 1998; FAO 2015). When considering 24-month rainfall accumulation periods, only the 1990-92 drought was more severe than the 2019-21 period (with ERA5 data dating back to 1950).

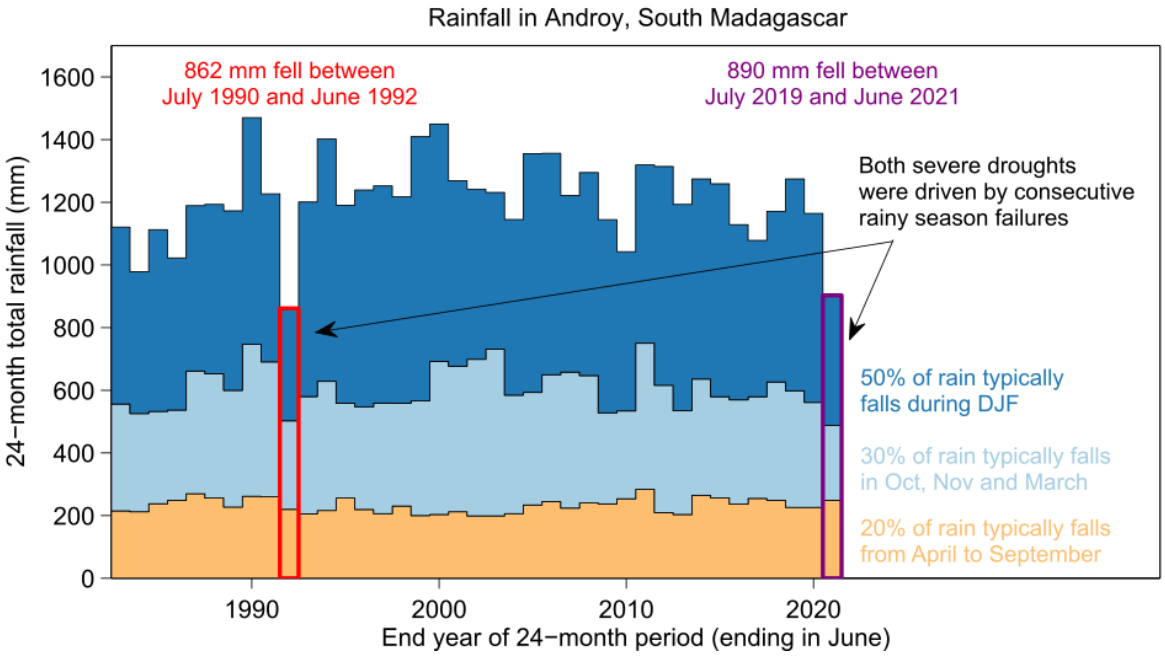

Figure 1: Schematic summary of recent 24-month rainfall totals averaged over the region of Androy in southern Madagascar, using CHIRPS rainfall data (via https://earlywarning.usgs.gov/fews/ewx/index.html). Coloured bars indicate which time of year is associated with different proportions of rainfall; the red and purple bars highlight the two worst rainfall deficits over a 24-month period on record: 1990-92 and the ongoing 2019-21 event.

1.1 Event impacts

Multiple organisations, in close partnership with the government of Madagascar, have established monitoring regimes relating to the ongoing risks of famine and food insecurity in the region: these organisations include the World Food Programme (WFP), The Famine Early Warning Systems Network (FEWS NET), the United Nations (via UNICEF, UNFPA, OCHA, FAO and others), and a multi-partner initiative, the Integrated Food Security Phase Classification group (IPC).

The IPC has performed in-depth analyses of ongoing food insecurity challenges in the southern regions of Madagascar since 2017, using a five-tier classification system (IPC 2021). In the second half of 2019, the fraction of people in Southern Madagascar classed as needing urgent assistance (Phase 3 or above) reached a low of 14%, in part due to more reliable rainfall patterns and improved harvests allowing a slow recovery from the impacts of previous drought in 2015/16. However, as both subsequent rainy seasons failed in 2019/20 and 2020/21, coupled with an array of compounding factors (see Section 7), an April 2021 assessment by the IPC found over 43% of the population (or 1.14 million people) are facing acute food insecurity challenges (Phase 3 or above), with tens of thousands classed as Phase 5 for the first time.

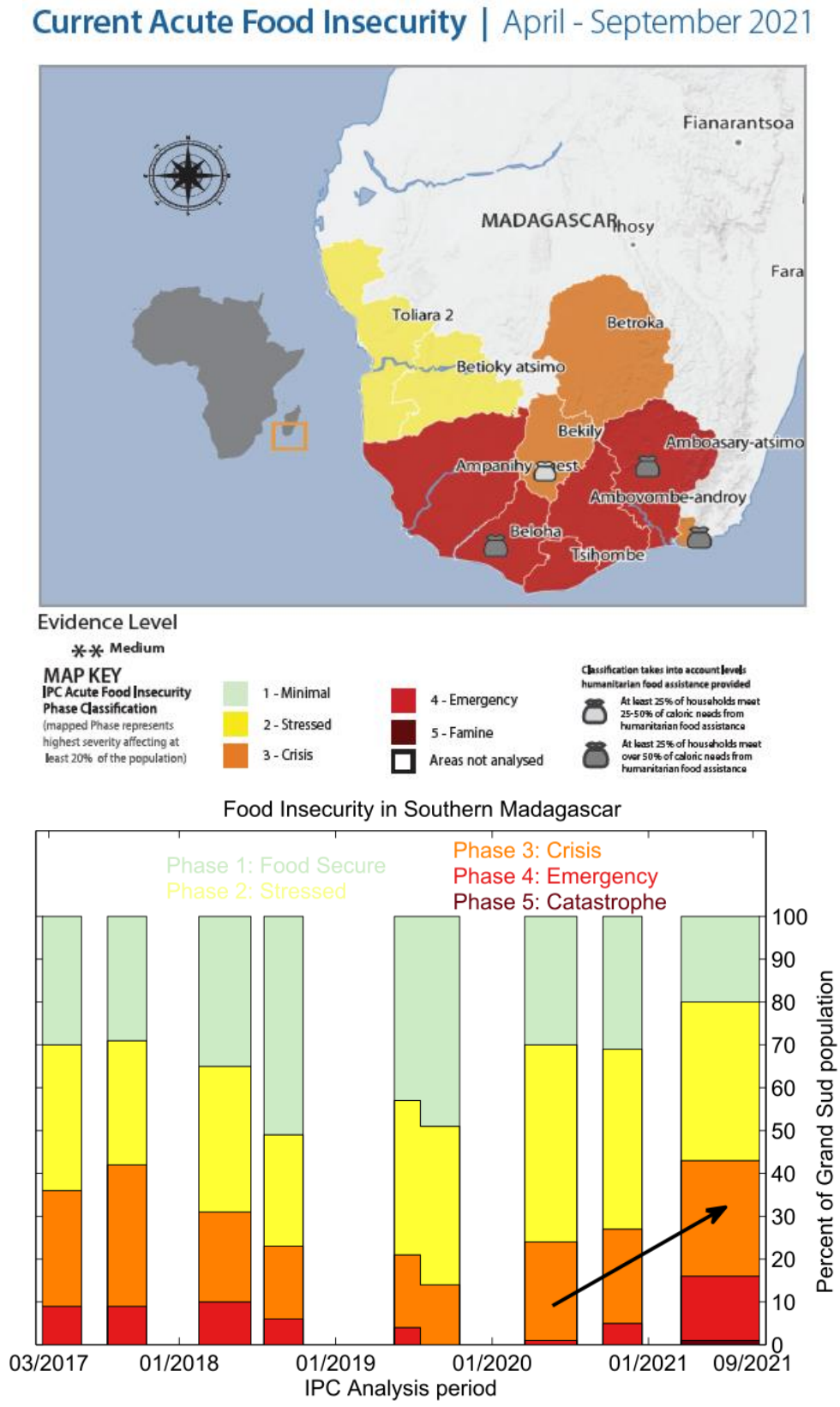

Figure 2: Top panel presents a map of the latest food insecurity situation over southern Madagascar (source: IPC 2021, https://bit.ly/3kQsKeT); a district is classified as Phase X when more than 20% of the local population is classified in that category or above. The bottom panel shows the time-evolution of food insecurity based on periodic IPC food insecurity analyses. The width of the bars show the period of time assessed by each individual IPC analysis. The black arrow highlights the rapid growth of severe food insecurity (Phase 3+) across the Grand Sud region over the last two years.

1.2 Event Definition

Droughts are comparably complex extreme events which depend on a number of climate and non-climate factors, as well as their interactions. Examples of the former include precipitation, temperature and soil- and vegetation-related feedbacks; examples of the latter include agricultural practices, the use of irrigation and choices around grazing density (van Loon et al., 2016). Accordingly, there are several definitions of drought in use, with meteorological drought (precipitation deficit), hydrological drought (low streamflow), agricultural and ecological drought (low soil moisture combined with high evaporative demand) being the most common (IPCC AR6 WG1 2021).

This complexity of drought poses challenges for their attribution, and in particular selecting the most appropriate event definition. With increasing temperatures, there is an *a priori* assumption that droughts are also becoming more severe. However, the link between droughts and climate change is often more complex: while agricultural and ecological droughts have increased in drought-prone areas like Southern Africa and the Mediterranean region, this is not the case for other types of drought nor for other arid regions, like Eastern Africa (Seneviratne et al., 2021). For Madagascar as a whole, Chapters 11 and 12 of the IPCC's Sixth Assessment Report (Seneviratne et al., 2021; Ranasinghe et al. 2021) determined with *medium confidence* that both meteorological and agro-ecological droughts will increase in response to global mean warming in excess of ~2°C, but a more regional assessment specifically for the Grand Sud has not been performed.

Importantly, Kew et al. (2021) systematically examined different methods of defining drought in the context of extreme event attribution for a sequence of both arid and semi-arid regions in East Africa, including those with a climate comparable to that of south-west Madagascar (Beck et al. 2018; see Appendix 1 for supporting details). The authors used a range of observational products, regional climate models, hydrological models and other impact models to explicitly decompose attributable changes in temperature, precipitation, evaporative demand and soil moisture associated with drought in a changing climate. Their results found that, while all analysed sub-regions did exhibit robust and statistically significant increases in temperature, this did not translate to corresponding increases in the likelihood of witnessing exceptional soil moisture deficits. Instead, they found that drought in these regions was primarily driven by precipitation deficits, while anomalously high temperatures did not necessarily exacerbate corresponding soil moisture anomalies. Such a result is supported by Manning et al. (2018), who found that the influence of precipitation on subsequent soil moisture deficits was much larger than that of temperature (via changes in evaporative demand) in water-limited observational settings.

Given these findings, the limited reliability of observations other than rainfall and temperature in this region, and the fact that precipitation deficits (i.e. meteorological drought) are used as a key determinant in regional drought forecasts and early warning systems, we focus on rainfall deficits in this analysis. Nevertheless, it is acknowledged that anomalously high temperatures in the area have almost certainly increased in frequency and intensity due to anthropogenic climate change: future studies employing appropriate modelling tools (including coupled hydrological models) to examine soil moisture changes directly over this region would therefore be useful to resolve the relationship between drought and temperature further.

Climatological Context:

The climate of Madagascar varies from humid tropical in the east to humid to semi-humid tropical over the central and western parts of the country, while the south is mainly semi-arid. The island is therefore characterized by strong East-West and North-South rainfall gradients. This spatial heterogeneity arises due to the complex interaction of different climate drivers across multiple scales, spanning from small-scale mesoscale processes to synoptic-scale teleconnections. The north-south mountain chain, reaching over 2600m in places and running along the eastern part of the island, interacts with moist air masses brought by the trade winds from the western Indian Ocean, leading to orographically enhanced rainfall year-round along the east coast. The mountains, on the other hand, act as a rain shadow for the western areas. The amount of rain in the east is therefore 2 to 3 times larger than that of the west (Jury et al., 1995).

DELIMITATION CLIMATIQUE DE MADAGASCAR

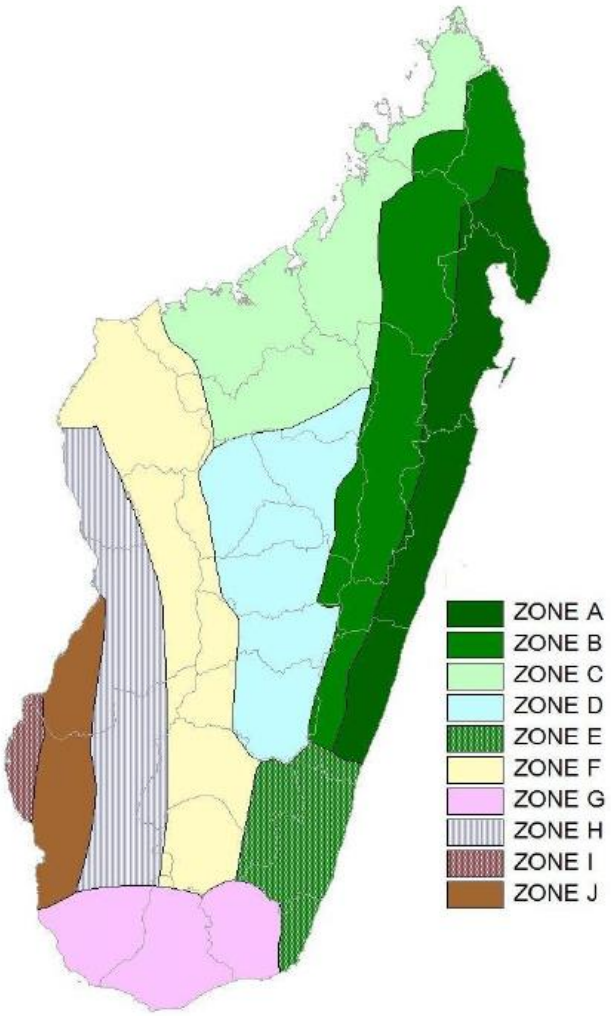

ZONES TRES HUMIDES

ZONE A : *Très humide toute l'année*
Exposée directement aux courants d'alizés.
Précipitation annuelle : 2500 - 3700 mm.
Température moyenne annuelle: ≥ 23,6°C.

ZONE B : *Très humide*
Influence des régimes d'alizé atténuée.
Précipitation annuelle : 1350 – 2500 mm.
Température moyenne annuelle : 18°C - 22°C.

ZONES HUMIDES

ZONE C : *Humide à forte pluviosité*
Exposée directement au régime de mousson en été.
Précipitation annuelle : 1200 – 2000 mm.
Température moyenne annuelle : ≥ 26°C.

ZONE D : *Humide*
Climat adouci par le relief ; pluie concentrée en été.
Précipitation annuelle : 1250 – 1500 mm.
Température moyenne annuelle : ≥ 19°C.

ZONE E : *Humide toute l'année*
Exposée directement au régime d'alizé.
Précipitation annuelle : 1400 – 1700 mm.
Température moyenne annuelle : ≥ 21°C.

ZONE F : *humideà faible précipitation*
Hiver sec.
Précipitation annuelle : 800 – 1100 mm.
Température moyenne annuelle : 18°C - 25°C.

ZONES SEMI HUMIDES

ZONE G : *semi humideventeux*
Influence des régimes d'alizé
Précipitation annuelle : 700 – 1200 mm.
Température moyenne annuelle : ≥ 23°C.

ZONE H : *semi humide*
Influence des effets locaux (brises).
Précipitation annuelle : 600 – 800 mm.
Température moyenne annuelle : ≥ 23°C.

ZONE I : *semi humide à faible pluviosité*
Précipitation annuelle : ~ 500 mm.
Température moyenne annuelle : ≥ 23°C.

ZONE SEMI ARIDE

ZONE J : *semi aride*
Nombre annuel de jours de pluie < 50.
Précipitation annuelle : < 500 mm.
Température moyenne annuelle : ≥ 22°C.

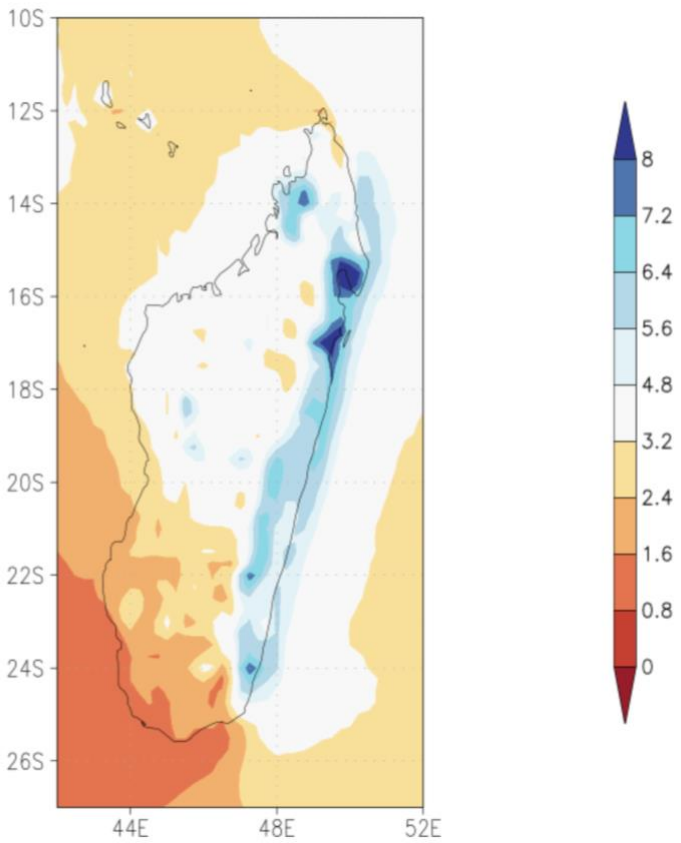

Figure 3: Top panel shows the classification of different climate zones, according to the 2014 Atlas Climatologique de Madagascar, issued by La Direction générale de la Météorologie (https://bit.ly/313Tty2). Bottom panel shows average annual rainfall (in units of mm/day) over 1951-2020, using data from ERA5.

Rainfall peaks during the austral summertime, enhanced by deep convection associated with tropical convergence: the southernmost position of Intertropical Convergence Zone establishes itself over the central part of the island (17-20°S) at the peak of the austral summer (Jury et al. 1995; Randriamahefasoa & Reason, 2017).

The northwestern part of the island receives summer rainfall primarily through NE monsoon winds originating from the western tropical Indian Ocean and recurving over the northern Mozambique Channel to become rain-bearing northwesterlies. The area is also characterized by rainfall from the strong mesoscale convective systems occurring in the northern Mozambique Channel. In addition, rainfall in the northern part of the island is also associated with low geopotential height over the southwestern Indian Ocean (Fauchereau et al. 2009; Jury, 2016). In contrast, rainfall in the southern region tends to be modulated by the Mozambique Channel Trough (Barimalala et al. 2018) and heavily influenced by less saturated air masses originating over the south-western Indian Ocean, with the south-west remaining mostly leeward and therefore relatively dry. Rainfall in the southern region is also driven by tropical temperate troughs - large convective systems linking the easterly subtropical wave to mid-latitude westerlies' frontal systems (Hart et al. 2013; Macron et al. 2016) - as well as cut-off lows (Favre et al., 2013; Hart et al. 2013).

Madagascar is also frequently affected by tropical cyclones (TCs) forming in the south-west Indian Ocean, although they mostly impact the East Coast of Madagascar. The south-west of the island is rarely impacted, although TC Favio in 2007 tracked close to the south and southwestern coasts

(Klinman & Reason 2008) and TC Dera in 2001 tracked southwards through the Mozambique Channel and passed close to the south-western coast of Madagascar (Reason 2007). In late January 2019, tropical storm Eketsang tracked along the south-western coast of Madagascar, delivering double the rainfall expected for that month across the region.

Spatial and Temporal Characteristics:

To determine the best choice of spatial domain for the attribution analysis requires a balance of multiple considerations, including where the impacts are most pronounced (section 1.1), differences in climate and land characteristics between different sub-regions of Madagascar (Figure 3), as well as the meteorological features of the drought itself.

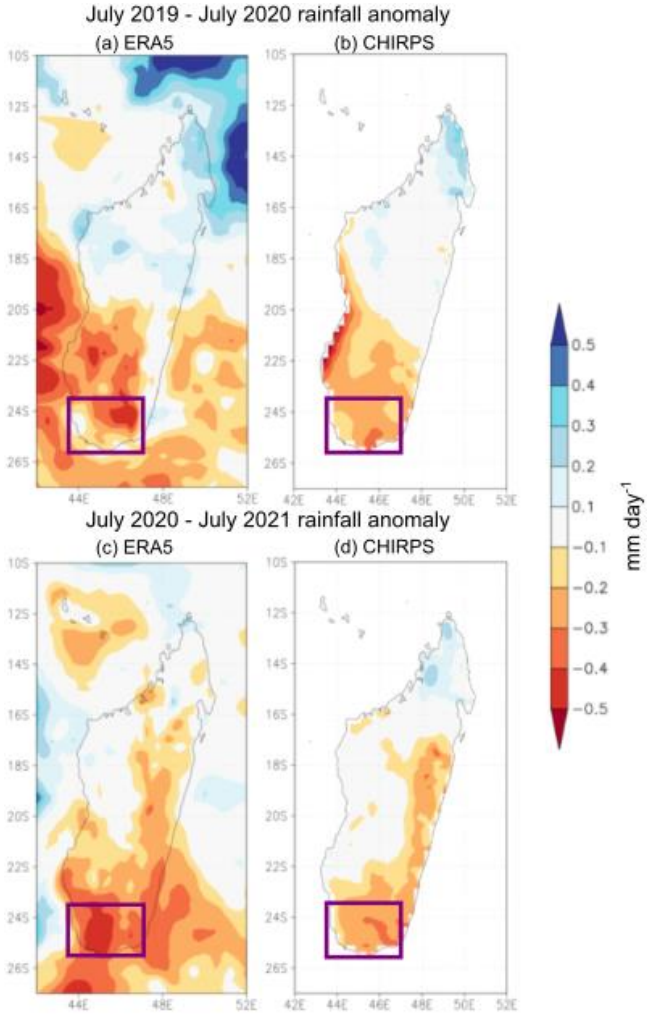

Figure 4: Maps of annual rainfall anomalies for two datasets (left-hand columns are ERA5; right-hand columns are CHIRPS) and for the twelve months of July 2019-June 2020 (top row) and July 2020-June 2021 (bottom row). Anomalies are presented in units of mm/day equivalents, relative to a 1991-2020 climatology, with the purple rectangle denoting the region selected for all subsequent analysis.

Looking first at the magnitude of rainfall deficits across the country using two different observation-related rainfall products (CHIRPS and ERA5; see section 2.1 for further details), Figure 4 confirms the southern regions of the country that have borne the worst humanitarian impacts of the drought are also those regions where annual rainfall deficits have been particularly severe for each of the last two years. Considering all lines of evidence together, and with a particular weight placed on the

concentrated humanitarian impacts in the very south of the country, we chose to hereafter define the spatial bounds of the drought event using latitude bounds of 23.5°S to 25.5°S and longitude bounds of 43.5°E to 47°E - this region is represented by the purple rectangles in the figure above, and is also referred to as the “Grand Sud” region in the remainder of the analysis.

Figure 5 then displays the time-evolution of recently-observed rainfall anomalies when averaging across this region of interest (where red and blue shading respectively indicates a drier-than-average and wetter-than-average month). There exists robust agreement across datasets of the following features: (1) the lack of rainfall during the last two wet seasons (and particularly the fourteen months spanning December 2019 to January 2021) has been particularly severe; (2) while January of 2019 represented an extremely wet month in the region, rainfall was also average throughout the entire 2018/19 hydrological year; and (3) the magnitude of any rainfall deficits during the rainy seasons of 2016/17 and 2017/18 were not considered significant, and likely counteracted by wetter-than-average shoulder seasons. For these reasons, coupled with the corresponding SPI calculations shown in panel c, we have chosen to define the length of the drought event as total rainfall for the 24-month period spanning July 2019 - June 2021 (inclusive).

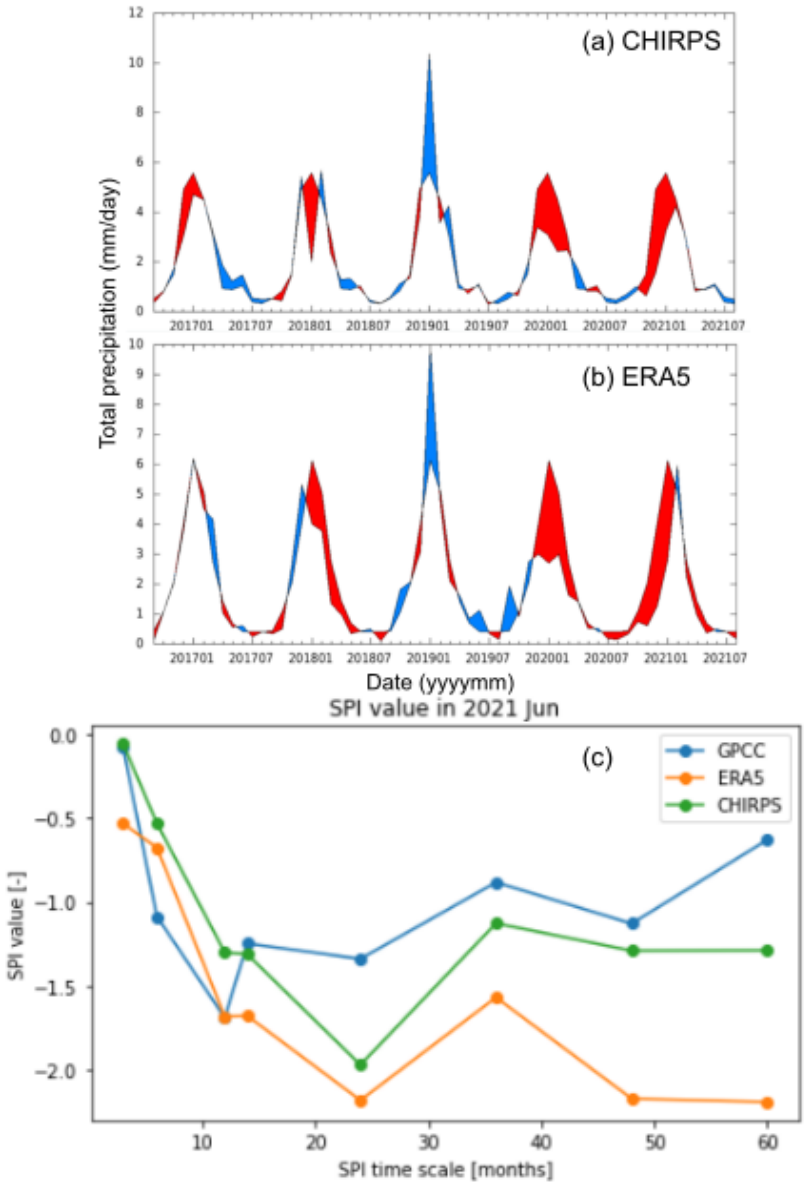

Figure 5: Contextualising the severity of the drought over Southern Madagascar when assessing different lengths of time. The top two panels show a time-series of monthly rainfall anomalies from CHIRPS and ERA5 data, where blue and red shaded areas respectively indicate positive and negative rainfall anomalies relative to a 1991-2020 climatology. The bottom panel considers the magnitude of rainfall deficits for a range of time-periods, all ending in June 2021: here, the relative severity magnitude of a rainfall deficit averaged over *n*-months (x-axis) is represented by the Standardised Precipitation Index, SPI.

1.3 Previous research

To our knowledge, there have been no attribution studies examining individual weather events over Madagascar. The IPCC Sixth Assessment Report classified the region as exhibiting "low confidence" of observed human influence on drought, "due to limited evidence". For those studies which have instead examined future projections of rainfall over the region, most generally conclude that annual mean rainfall is projected to decrease under moderate- and high-emissions climate scenarios, but this signal of change has yet to emerge from the 'noise' of internal variability in the current climate.

Historical trends:

Randriamarolaza et al. (2021) examined observed trends from 28 weather stations across the country, and found observed decreases in rainfall in some stations across Madagascar and corresponding increases in drought-related indices. However, trends were largely statistically insignificant and no station data were available over the Grand Sud region most affected by the ongoing food security crises. Our analysis of data from the nearest available weather stations in GHCN-D (see Appendix 2) found large data gaps which prevented any complementary analysis of observed rainfall trends.

Lim Kam Sian et al. (2021) found no statistically significant trends in observed rainfall from 1900 to 2014, when considering the months of May to October and November to April individually for both observation-derived rainfall datasets (GPCC, CRU and UDel) and corresponding CMIP6 model simulations.

Synthesizing the evidence of rainfall and drought trends for Madagascar as a whole, including assessments relating to dry-season water availability by Padrón et al (2020), Seneviratne et al. (2021) concluded there were no consistent trends of observed changes in drought over the region.

Future projections:

Lim Kam Sian et al. (2021) examined twenty-first century projections of seasonal rainfall change in CMIP6 models under medium- and high-warming scenarios (SSP2-4.5 and SSP5-8.5). While any projected changes in wet-season (DJFM) rainfall were statistically insignificant, trends of decreasing May-October rainfall were found to emerge across Madagascar in the second half of the twenty-first century under an SSP5-8.5 scenario, with drying signals more evident over the east of the country.

Coppola et al. (2021) examined future changes in the frequency of meteorological drought events over Madagascar for a range of different climate model experiments and scenarios, including high- and low-emission scenarios from CMIP5, CMIP6 and multiple CORDEX regional model experiments. The authors focused on the Standardised Precipitation Index for a time window of six months (SPI-6) and chose to define a drought as starting in any month when SPI-6 falls below 1, and ending when SPI-6 returned to positive values for at least two corresponding months. When defined in this manner, Coppola and colleagues found most models to overestimate observed drought frequency (identifying

2-3 events per decade instead of the observed 1-2), while best-guess estimates across all model ensembles projected an additional one to two droughts per decade by mid-century. Using the same index, the IPCC (2021, Chapter 12, Figure 4) found a consistent increase in the number of drought events across model ensembles (CMIP5, CMIP6 and CORDEX) by late-century under RCP8.5 or SSP5-8.5.

Barimalala and colleagues (2021) presented a comprehensive analysis of projected climate changes under 1.5 and 2 degrees of warming specifically for Madagascar, using regional climate models from the CORDEX-Africa ensemble. Robust decreases in rainfall were projected for northern and eastern parts of the country during the months of October to December at these thresholds of future warming, while statistically insignificant changes were projected for the southern and western regions of the country currently experiencing ongoing drought impacts. This spatial heterogeneity is in agreement with Lim Kam Sian et al. (2021), offering important context when interpreting country-level syntheses seen elsewhere, like the Interactive Atlas of the IPCC Sixth Assessment Report (https://interactive-atlas.ipcc.ch/regional-information). The authors also report mostly non-significant increases in rainfall during the wetter months of January to April across the country, with more pronounced increases again in the north and east of the country.

Dosio et al. (2019) also performed an in-depth assessment of the significance and robustness of future changes in both mean rainfall as well as extreme precipitation-related indices over the country, albeit analysing end-of-century (2081-2100) simulations from CORDEX-Africa under a high-warming RCP8.5 scenario. They confirmed the results of previous work, showing that high levels of global warming lead to robust projected reductions in season mean rainfall over SON (particularly eastern and northern regions) and smaller but statistically significant increases in rainfall during DJF. Robust increases in both the intensity of extreme wet days and in the frequency of consecutive dry days were also reported, with these extreme indices showing larger signals of change than in the mean.

Finally, Kendon et al. (2019) examined end-of-century (under RCP8.5) changes in wet-season rainfall characteristics over the African continent, using a 4.5-km resolution convection-permitting climate model. Results show evidence of statistically significant increases in wet-season mean rainfall over southwestern Madagascar in a high-warming scenario, with changes being largely driven by corresponding increases in the intensity of the most extreme rainfall events.

Combined, previous research suggests that future warming over the twenty-first century could lead to small-to-moderate increases in wet-season rainfall over southern Madagascar (largely driven by the intensification of the wettest days of the year), while the latter half of the dry season (August-October) is projected to become drier and longer. The sign of change is mostly consistent across Madagascar, although the magnitude of these relative changes are more pronounced in northern and eastern regions. Most modelling studies further suggest that such changes - as well as corresponding signals of change in average rainfall over one or two consecutive years - are unlikely to be statistically significant (or have “emerged” from the “noise” of internal variability) after only 1.2°C of global temperature rise.

2. Data and methods

2.1 Observational data

Several options exist when evaluating a recent extreme weather event in the context of historical climate observations. While analyzing historical data from local weather stations is the first preference for any study, we found no station data of sufficient quality within the region of interest, having evaluated available station data within the TAHMO, GHCN and CRU datasets (see Appendix for further details).

Rainfall data from "Climate Hazards Group InfraRed Precipitation with Station data" (CHIRPS; Funk et al. 2015) is frequently used for analyses over the Southern Africa region (including by FEWS NET for their food insecurity projections) and was thus considered for our analysis. However, due to the relatively short length of the CHIRPS dataset (dating back to 1981) we restrict our use of the CHIRPS dataset to only examining the characteristics of the event and comparing with other datasets: the length of the CHIRPS dataset does not, for example, allow us to successfully fit a Generalised Pareto Distribution (GPD) with only the lowest 20% of data (see Section 2.3 for an explanation).

Because we were interested in analysing time-series which are as long as possible, we have also examined precipitation data from the European Centre for Medium-Range Weather Forecasts via their ERA5 reanalysis product (which dates back to 1950; Hersbach et al. 2020). Figure 7 presents statistical characteristics of the two datasets over the Grand Sud region of Madagascar, revealing good agreement on both seasonal rainfall characteristics as well as on the timing of past drought events.

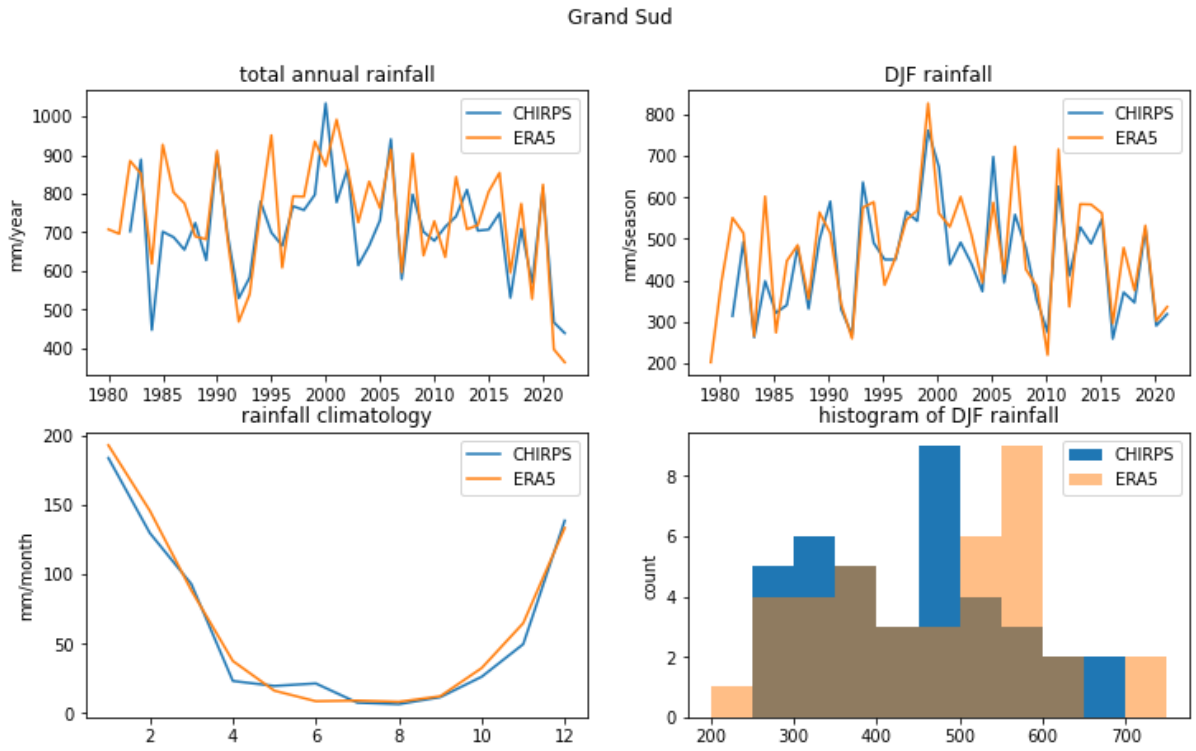

Figure 6: Comparing ERA5 and CHIRPS rainfall statistics over the southernmost region of Madagascar (Grand Sud region).

As a measure of anthropogenic climate change, we use the (low-pass filtered) global mean surface temperature (GMST), where GMST is taken from the National Aeronautics and Space Administration (NASA) Goddard Institute for Space Science (GISS) surface temperature analysis (GISTEMP, Hansen et al., 2010 and Lenssen et al. 2019).

2.2 Model and experiment descriptions

For the attribution of the drought event, three different model ensembles are used.

The first is the CORDEX-Africa (0.44° resolution, AFR-44) multi-model ensemble (Nikulin et al., 2012). The ensemble used consists of 22 simulations resulting from pairings (as of November 2021) of Global Climate Models (GCMs) and Regional Climate Models (RCMs) (see the table below). These simulations are composed of historical simulations up to 2005 and then extended to the end of the 21th century using the RCP8.5 scenario. For each simulation, we consider the entire period available for attribution. All models were tested for the GPD parameters against observations and one model was removed because the 95% confidence intervals were not overlapping with the ERA5 confidence intervals.

RCM	GCM	Years
RCA4	CanESM2	1951-2099
	EC-EARTH	1951-2099
	CNRM-CM5	1951-2099
	HadGEM2-ES	1951-2098
	MPI-ESM-LR	1951-2099
	IPSL-CM5A-LR	1951-2099
	CSIRO-Mk3-6-0	1951-2099
	NorESM1-M	1951-2099
	MIROC5	1951-2099
	GFDL-ESM2M	1951-2099
CCLM4-8-17	CNRM-CM5	1950-2099
	HadGEM2-E	1949-2097
	EC-EARTH	1949-2098
	MPI-ESM-LR	1949-2098
HIRHAM5	EC-EARTH	1951-2099
RACMO22T	EC-EARTH	1950-2099
	HadGEM2-ES	1950-2098
REMO2009	EC-EARTH	1950-2099
	HadGEM2-ES	1950-2098
	MPI-ESM-LR	1950-2099
	IPSL-CM5A-LR	1950-2099
	MIROC5	1950-2099

Table 1: List of the RCMs used with their driving GCMs and the period simulated (see Nikulin et al. (2012) for a description of the RCMs and Taylor et al. (2012) for the GCMs). The RCA4 downscaling MIROC5 was removed after model evaluation.

The second ensemble is the HighResMIP SST-forced model ensemble (Haarsma et al. 2016), spanning 1950-2050. For the 'present' time period (1950-2014), the SST and sea ice forcings used in the HighResMIP are based on the daily, 0.25° x 0.25° Hadley Centre Global Sea Ice and Sea Surface Temperature dataset, with area-weighted regridding used to map this to each model grid. For the 'future' time period (2015-2050), SST/sea-ice data are derived from RCP8.5 (CMIP5) data, and combined with greenhouse gas forcings from SSP5-8.5 (CMIP6) simulations (see Section 3.3 of Haarsma et al. 2016 for further details). For each simulation, we consider the time period up to the event (1950-2021) for attribution. We also tested using the entire time period (1950-2050) to increase the sample size, though this sensitivity test yielded negligible differences in the final results (not shown).

For HighResMIP, only those models with a spatial resolution comparable with ERA5 and CHIRPS are considered in this analysis, with one ensemble member used from each model:

HiResMIP model	**Institution**	**Horizontal resolution**

CNRM-CM6-1-HR	Centre National de Recherches Meteorologiques	~50km
EC-Earth3P-HR	EC-Earth-Consortium	~40km
HadGEM3-GC31-HM	Met Office Hadley Centre	~25km
CMCC-CM2-VHR4	Fondazione Centro Euro-Mediterraneo sui Cambiamenti Climatici	~25km
MPI-ESM1-2-XR	Max Planck Institute for Meteorology	~60km

Table 2: List of five climate models analysed from the HiResMIP SST-forced experiment, including their spatial resolution.

We also use five ensemble members of simulations from both the AM2.5C360 (Yang et al. 2021, Chan et al. 2021) and FLOR (Vecchi et al. 2014) climate models developed at Geophysical Fluid Dynamics Laboratory (GFDL). AM2.5C360 is an atmospheric GCM with a horizontal resolution of 25 km. Its five ensemble simulations are AMIP experiment (1871-2021) initialized from five different pre-industrial conditions but forced by the same SSTs from HadISST1 (Rayner et al. 2003) after groupwise adjustments (Chan et al. 2021), as well as the same historical radiative forcings. The FLOR model, on the other hand, is an atmosphere-ocean coupled GCM with a resolution of 50 km for land and atmosphere and 1 degree for ocean and ice. The five ensemble simulations cover the period from 1860 to 2100 and include both the historical and RCP4.5 experiments driven by transient radiative forcings from CMIP5 (Taylor et al. 2012).

2.3 Statistical methods

In this analysis we examine 24-month running mean rainfall data (from July to June), averaged over the southern Madagascar region (as defined in Section 1.2). Methods for observational and model analysis and for model evaluation and synthesis are used according to the World Weather Attribution Protocol, described in Philip et al. (2020), with supporting details found in van Oldenborgh et al. (2021), Ciavarella et al. (2021) and here.

The analysis steps include: (i) trend calculation from observations; (ii) model evaluation; (iii) multi-method multi-model attribution and (iv) synthesis of the attribution statement.
We calculate the return periods, Probability Ratio and change in intensity of the event in question when comparing observed GMST values of 2021 with past GMST values (1850-1900, based on the Global Warming Index https://www.globalwarmingindex.org), an estimated difference of 1.2°C.

To statistically model the event in question, we adopt the approach of Kew et al. (2021) and references therein, using a Generalised Pareto Distribution (GPD) that scales with GMST, and fitted to the lowest 20% of the data to focus on low precipitation extremes. When scaling with GMST as a covariate, the location and scale parameters are both adjusted, such that the ratio of the two (i.e. the dispersion parameter) remains unchanged. To account for the autocorrelation associated with the 2-year running mean, the error margins associated with the GPD fit were computed with a moving block bootstrap with a block size of 2 years.

Finally, results from observations and models that pass the validation tests (see Section 4) are synthesized into a single attribution statement.

3. Observational analysis: return time and trend

3.1 Analysis of gridded data

Figure 7 shows a time-series of annual rainfall for the two observational datasets considered. As explained in Section 2.1, we only examine warming-related trends in rolling 24-month rainfall accumulations with the ERA5 data, as the length of the CHIRPS data is too short to meet the statistical requirements for a GPD-based analysis.

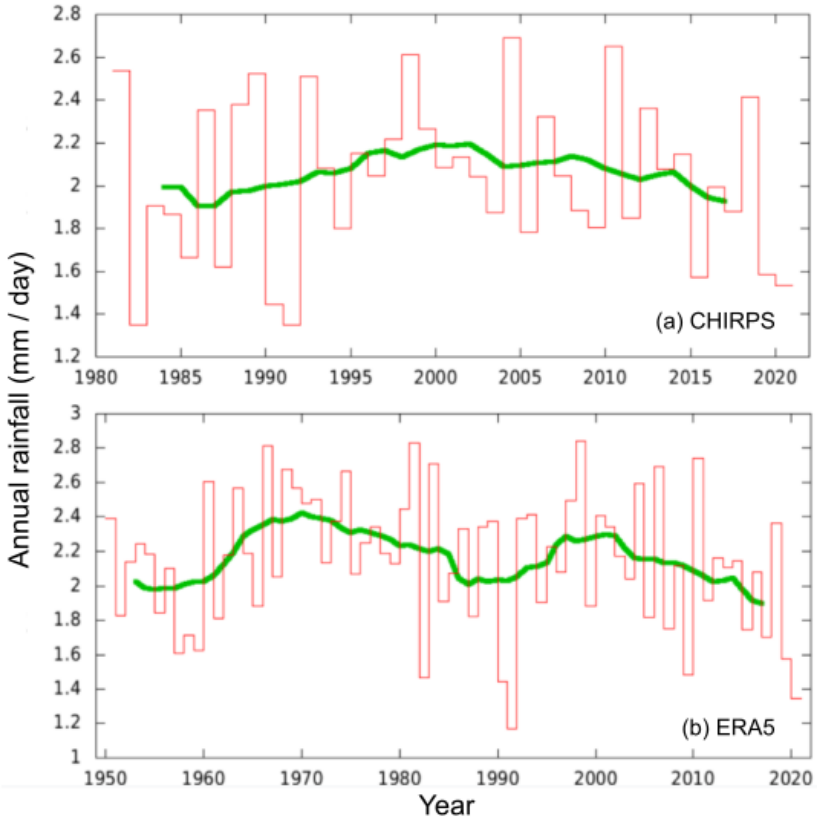

Figure 7: Time series of annual rainfall accumulations (July to June) over southern Madagascar using (a) CHIRPS and (b) ERA5 rainfall data, along with a ten-year running mean (green line). The x-axis denotes the end year of the July-to-June period considered.

Figure 8 presents the trend fitting methods applied to the ERA5 transient series and time slices, respectively. In the top panel, The thick red line denotes the location parameter scaled with GMST, while the thin red lines denote the corresponding 6- and 40-yr return levels of low-rainfall anomalies. The bottom panel presents return time plots for the climate of 2021 (red) and a climate with GMST 1.2 ºC cooler. The magenta horizontal line indicates the average daily-mean rainfall observed across the 24 months of the 2019-21 drought: rainfall deficits of this magnitude correspond to a best-guess return period of 1-in-135 years in today's climate (the intersection of the middle red line), albeit with high levels of uncertainty (the outer red lines).

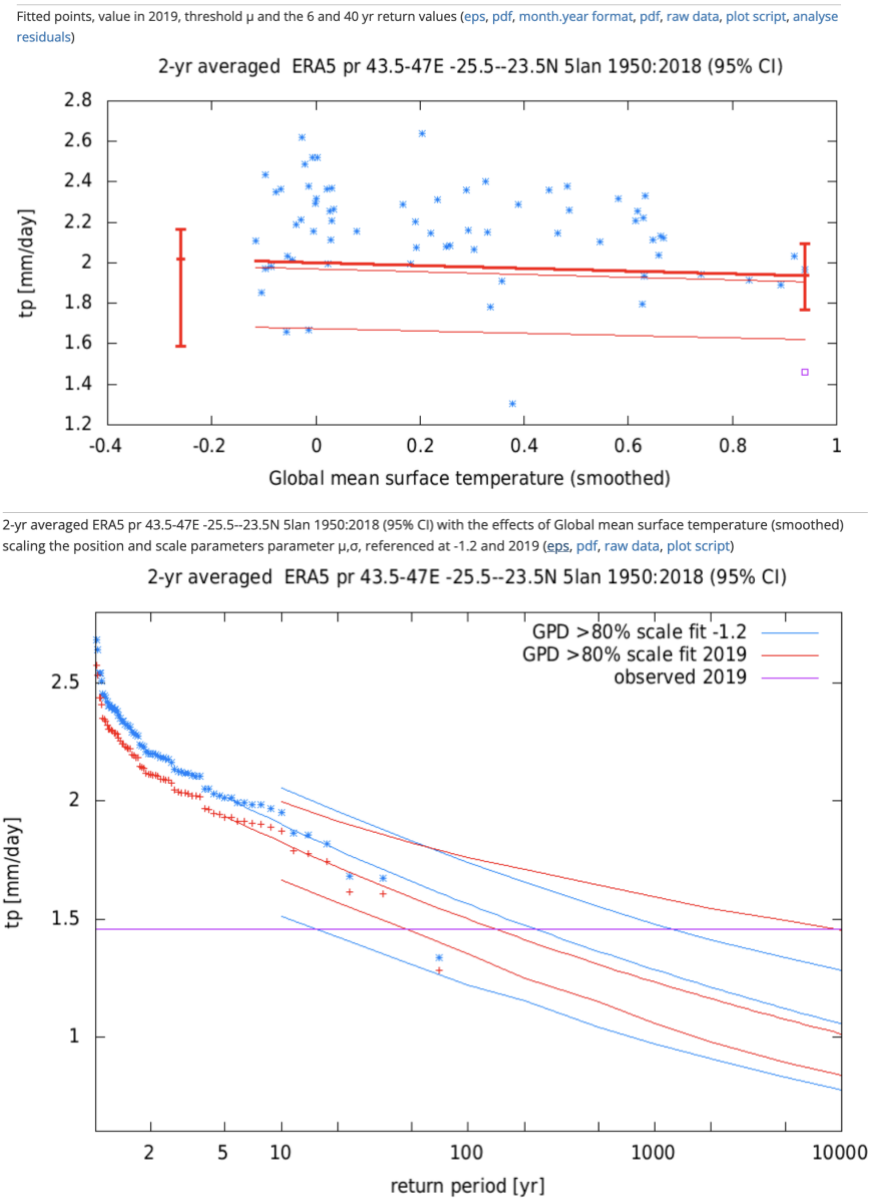

Figure 8: GPD fit with constant dispersion parameters, and location parameter scaling proportional to GMST of the index series. No information from 2021 is included in the fit. **Top**: Observed 24-month running precipitation totals as a function of the smoothed GMST. The thick red line denotes the location parameter, the thin red lines the 6- and 40-yr return levels. The 2019-2021 drought observation is highlighted with the magenta box. **Bottom:** Return time plots for the climate of 2021 (red) and a climate with GMST 1.2 ºC cooler (blue). The past observations are shown twice: once shifted up to the current climate and once shifted down to the climate of the late nineteenth century. The magenta line shows the magnitude of the 2019-21 event analysed here.

3.2 Influence of modes of natural variability

Wet-season precipitation is highly variable over southern Madagascar, as shown in the top-right panel of Figure 6. Several modes of natural climate variability are known to modulate seasonal rainfall over the wider southern Africa region, including the El Niño Southern Oscillation (ENSO), the Indian Ocean Dipole (IOD) and the sub-tropical Indian Ocean Dipole (sIOD) (Hoell et al. 2015, 2017; Hart et al. 2018). However, the extent to which these modes of variability represent a causal driver of the recent rainfall deficits over southern Madagascar remains less clear.

Generally speaking, the majority of impacts driven by significant Indian Ocean Dipole "events" occur well to the north of Madagascar - they can be significant over the Horn of Africa, for example (see Figure 9 below; Cai et al. 2021; Figure 1b from Abram et al. 2020). While the months of October to November 2019 did mark the peak of a severe positive IOD event, rainfall was mostly average over southern Madagascar until later in December that year. Moreover, there were also significant IOD events in 1994, 1997 and 2006 (Cai et al. 2021), none of which aligned with significant drought events over southern Madagascar.

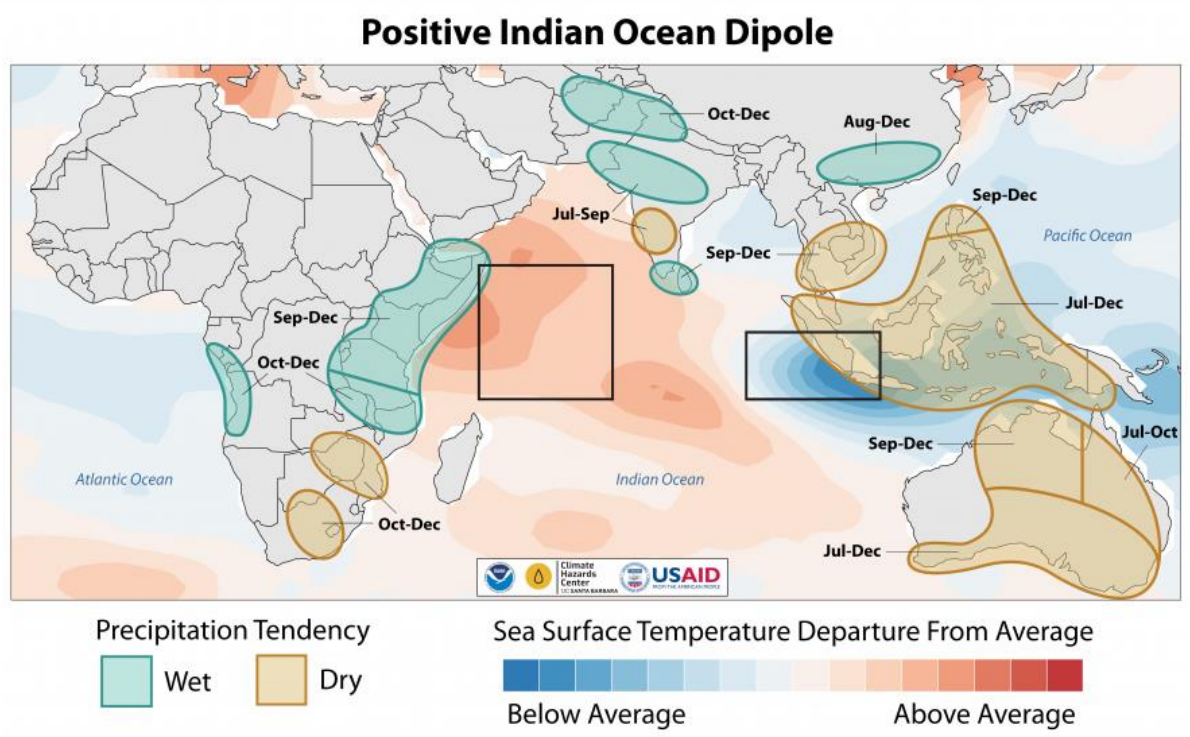

Figure 9: Schematic illustrating the timing of wet and dry conditions related to positive Indian Ocean Dipole events. SOURCE: https://fews.net/indian-ocean-dipole-and-precipitation.

When examining the relationship between NINO3.4 index and DJF rainfall globally (using ERA5), a statistically significant relationship between ENSO and seasonal rainfall was found over both Southern Africa and Eastern Africa, with El Niño events aligning with low- and high-rainfall anomalies, respectively (see Figure 10 below). However, the strength of this correlation was less significant over southern Madagascar, with similarly weak results also found when looking instead over the months of September to November or when considering GPCC rainfall data (not shown).

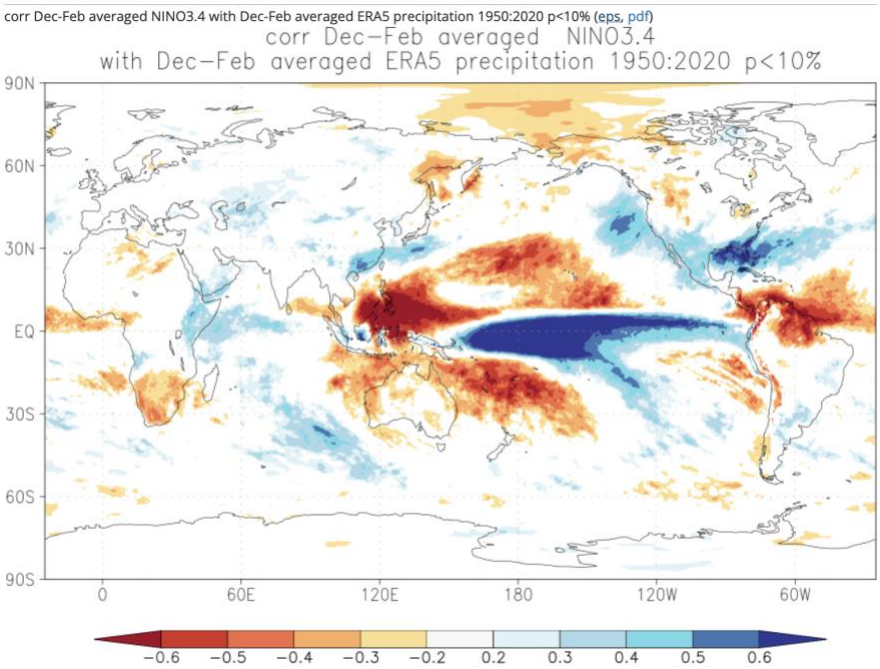

Figure 10: ENSO-rainfall relationships for DJF, using data from ERA5. Blue colours indicate that during El Niño there was, on average, more rain than normal, red colours indicate drought during El Niño. La Niña has the opposite effect in almost all locations. As a measure of the strength of the relationship we used the correlation coefficient with the Niño3.4 index. The square of this number gives the fraction of the variance that is explained by this aspect of El Niño.

Past instances of back-to-back precipitation deficits during the rainy season (1990-92) have coincided with moderate-strong El Niño events, as did the dry summer of 2015/16. Hoell et al. (2017) suggests, for example, that an El Niño event aligning with an opposite-signed sIOD phase offers good predictability of low rainfall over the region in question. However, such criteria were indeed met during the severe El Niño of 1997/98 and yet coincided with a normal rainy season over southern Madagascar. Moreover, the back-to-back poor rainy seasons in 2008-10 alternated between positive and negative ENSO phases, while the extremely dry summer of 2020/21 coincided with a moderate-strength La Niña event (the summer of 2019/20 was ENSO-neutral).

Altogether, external modes of variability appear to have played little if any role in the formation of the event.

4. Model evaluation

In this section we show the results of the model evaluation. Three evaluation criteria are applied: an assessment of the similarity between the modelled and observed seasonal cycle of rainfall over the region (as exemplified by the results for the HighResMIP models in Figure 11, below); a qualitative check of the spatial pattern of climatological rainfall across Madagascar, and a test of the dispersion and shape parameters of the GPD distribution (where the dispersion parameter is defined as the ratio of the scale and location parameter, σ/μ). This combined assessment results in each model being classified as either "good", "reasonable" or "bad", according to the criteria defined in Ciavarella et al. (2021). In this study, we use models that are labelled "good" or "reasonable" for subsequent analysis.

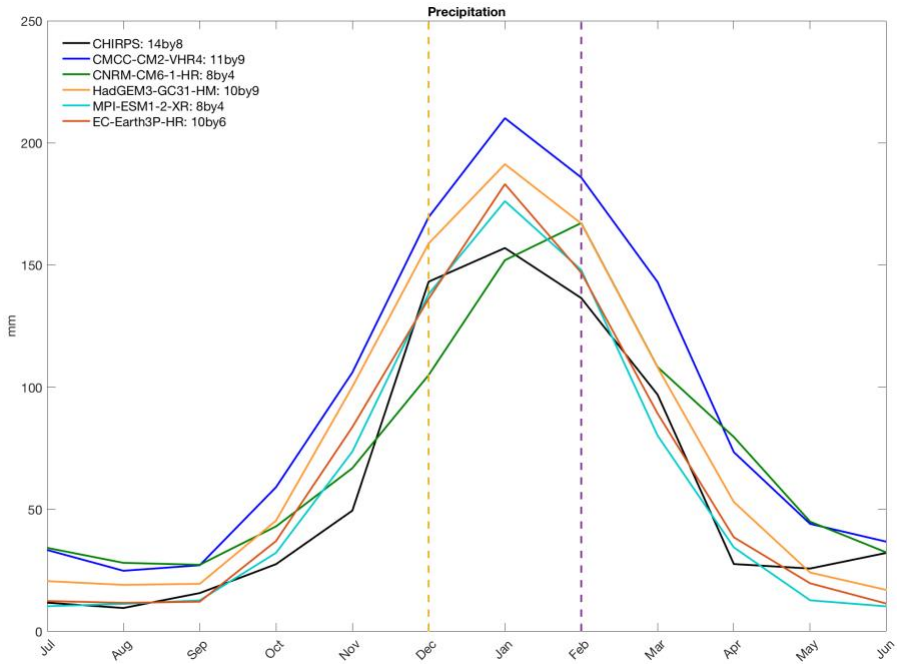

Figure 11: Seasonal cycle of monthly precipitation simulated by the five HighResMIP models (coloured lines) compared with corresponding CHIRPS observations (black) over the region of interest in Southern Madagascar.

Table 1 shows the model evaluation results, including both the models that passed the evaluation tests (labelled as "good" or "reasonable") and models which did not (labelled as "bad"). Of those models considered, CMCC-CM2-VHR4, CNRM-CM6-1-HR and RCA4-MIROC5 were labelled as “bad” and discarded from the subsequent attribution analysis, primarily because the 95% confidence intervals of the GPD parameters did not overlap with the corresponding ERA5 confidence intervals. We also note that, due to the shorter time series length, values for CHIRPS in Table 1 are calculated using the lowest 30% of precipitation in the GPD fit rather than the lowest 20% and therefore cannot be directly compared to the other values.

Model / Observations	**Seasonal cycle**	**Spatial pattern**	**Dispersion**	**Shape parameter**	**Conclusion**
ERA5			0.0850 (0.0450 ... 0.112)	-0.085 (-0.12 ... -0.049)	
CHIRPS (lowest 30%)			0.0800 (0.0500 ... 0.106)	-0.080 (-0.11 ... -0.050)	
RCA4/CanESM2	good	reasonable	0.144 (0.0670 ... 0.200)	-0.35 (-0.61 ... -0.069)	reasonable
RCA4/EC-EARTH	good	reasonable	0.0790 (0.0450 ... 0.120)	-0.27 (-0.56 ... -0.046)	reasonable
RCA4/CNRM-CM5	good	reasonable	0.0610 (0.0420 ... 0.0960)	-0.13 (-0.43 ... -0.042)	reasonable
RCA4/ HadGEM2-ES	good	reasonable	0.114 (0.0570 ... 0.209)	-0.58 (-1.1 ... -0.060)	reasonable
RCA4/ MPI-ESM-LR	good	reasonable	0.0880 (0.0420 ... 0.137)	-0.35 (-0.67 ... -0.043)	reasonable
RCA4/IPSL-CM5A-LR	good	reasonable	0.0850 (0.0590 ... 0.190)	-0.13 (-0.58 ... -0.060)	reasonable
RCA4/CSIRO-Mk3-6-0	good	reasonable	0.110 (0.0470 ... 0.150)	-0.34 (-0.63 ... -0.047)	reasonable

RCA4/NorESM1-M	good	reasonable	0.170 (0.0830 ... 0.185)	-0.55 (-0.69 ... -0.086)	reasonable
RCA4/MIROC5	good	reasonable	0.191 (0.110 ... 0.230)	-1.1 (-1.3 ... -0.51)	bad
RCA4/GFDL-ESM2M	good	reasonable	0.120 (0.0540 ... 0.190)	-0.39 (-0.84 ... -0.055)	reasonable
CCLM4-8-17/CNRM-CM5	good	good	0.0810 (0.0690 ... 0.0760)	-0.087 (-0.078 ... -0.078)	good
CCLM4-8-17/EC-EARTH	good	good	0.110 (0.0950 ... 0.100)	-0.12 (0.11 ... 0.11)	reasonable
CCLM4-8-17/HadGEM2-ES	good	good	0.0780 (0.0680 ... 0.120)	-0.090 (-0.18 ... -0.081)	good
CCLM4-8-17/MPI-ESM-LR	good	good	0.140 (0.0590 ... 0.290)	-0.47 (-1.2 ... -0.060)	reasonable
HIRHAM5/EC-EARTH	good	reasonable	0.0740 (0.0360 ... 0.112)	-0.15 (-0.46 ... -0.038)	reasonable
RACMO22T/EC-EARTH	good	good	0.0790 (0.0440 ... 0.120)	-0.11 (-0.51 ... -0.045)	good
RACMO22T/ HadGEM2-ES	good	good	0.0660 (0.0350 ... 0.104)	-0.14 (-0.48 ... -0.037)	reasonable
REMO2009 /EC-EARTH	good	good	0.150 (0.0590 ... 0.160)	-0.41 (-0.55 ... -0.059)	reasonable
REMO2009 / HadGEM2-ES	good	good	0.155 (0.0790 ... 0.262)	-0.32 (-0.79 ... -0.079)	reasonable
REMO2009 / MPI-ESM-LR	good	good	0.110 (0.0500 ... 0.270)	-0.37 (-1.1 ... -0.050)	reasonable
REMO2009 /IPSL-CM5A-LR	good	good	0.159 (0.0700 ... 0.311)	-0.42 (-1.1 ... -0.070)	reasonable
REMO2009 /MIROC5	good	good	0.0830 (0.0380 ... 0.110)	-0.18 (-0.52 ... -0.039)	reasonable
HadGEM3-GC31-HM HighresMIP	good	good	0.0740 (0.0380 ... 0.0810)	-0.074 (-0.14 ... -0.038)	good
EC-Earth3P-HR HighresMIP	good	good	0.0330 (0.0130 ... 0.0510)	-0.081 (-0.21 ... -0.015)	reasonable
CNRM-CM6-1-HR HighresMIP	reasonable	good	0.0350 (0.0160 ... 0.0320)	-0.035 (-0.041 ... -0.017)	bad
CMCC-CM2-VHR4 HighresMIP	good	reasonable	0.0390 (0.0330 ... 0.0450)	-0.039 (-0.12 ... -0.035)	bad
MPI-ESM1-2-XR HighresMIP	good	reasonable	0.0490 (0.0200 ... 0.0800)	-0.22 (-0.23 ... -0.021)	reasonable
GFDL/AM2.5C360	good	reasonable	0.0750 (0.0560 ... 0.0900)	-0.22 (-0.40 ... -0.059)	reasonable
FLOR	good	good	0.0720 (0.0570 ... 0.0880)	-0.19 (-0.35 ... -0.061)	reasonable

Table 3: List of the model validation procedures applied, along with a corresponding assessment of overall suitability for attribution analysis (final column). Observations in blue, models in black.

5. Multi-method multi-model attribution

Here, we calculate the probability ratio, as well as the change in magnitude of the event, in both the observations and the models. For each model considered, we focus on the change in frequency and

intensity associated with a 1-in-135 year event (which was the best estimate of the observed event's rarity) as defined within that model. Only models which passed the validation tests in Section 4 are presented below.

Table 4 shows the probability ratios and change in intensity for ERA5, CHIRPS and for the models that passed our validation tests (see Table 3). Note again that values for CHIRPS in Table 4 are calculated using the lowest 30% of precipitation in the GPD fit rather than the lowest 20% and therefore cannot directly be compared to the other values. In the synthesis (Section 6), we therefore only include ERA5 and not CHIRPS.

Model / Observations	**Threshold for return period 135 yr**	**Probability ratio PR [-]**	**Change in intensity ΔI [%]**
ERA5	1.46 mm/day	1.6 (0.0064 ... 5.4)	-4.1 (-14 ... 30)
CHIRPS lowest 30%. Not used for validation.	1.56 mm/day	6.1 (0.021 ... 30)	-13 (-22 ... 38)
RCA4/CanESM2	0.90 mm/day	2.1 (0.93 ... ∞)	-4.2 (-15 ... 0.46)
RCA4/EC-EARTH	1.7 mm/day	0.64 (0.37 ... 17)	1.8 (-5.7 ... 4.2)
RCA4/CNRM-CM5	2.4 mm/day	0.50 (0.019 ... 0.88)	3.4 (0.59 ... 7.1)
RCA4/ HadGEM2-ES	1.8 mm/day	0.58 (0.12 ... 9.2)	1.3 (-3.4 ... 6.6)
RCA4/ MPI-ESM-LR	1.9 mm/day	1.0 (0.44 ... ∞)	-0.048 (-9.4 ... 2.9)
RCA4/IPSL-CM5A-LR	1.5 mm/day	0.35 (0.12 ... 2.6)	8.0 (-4.1 ... 10)
RCA4/CSIRO-Mk3-6-0	0.90 mm/day	7.2 (1.5 ... ∞)	-6.7 (-14 ... -2.5)
RCA4/NorESM1-M	1.2 mm/day	3.8 (0.53 ... ∞)	-3.5 (-14 ... 3.3)
RCA4/GFDL-ESM2M	1.9 mm/day	4.3 (0.50 ... ∞)	-4.5 (-8.3 ... 3.6)
CCLM4-8-17/CNRM-CM5	1.2 mm/day	1.1 (0.91 ... 1.4)	-0.73 (-2.2 ... 0.66)
CCLM4-8-17/EC-EARTH	0.70 mm/day	2.0 (1.8 ... 2.6)	-6.6 (-8.5 ... -5.0)
CCLM4-8-17/HadGEM2-ES	0.70 mm/day	2.3 (1.4 ... 3.2)	-6.0 (-7.7 ... -2.4)
CCLM4-8-17/MPI-ESM-LR	0.90 mm/day	1.8 (0.59 ... ∞)	-2.1 (-12 ... 3.1)
HIRHAM5/EC-EARTH	1.4 mm/day	2.9 (1.8 ... ∞)	-5.6 (-12 ... -2.3)
RACMO22T/EC-EARTH	1.1 mm/day	1.4 (0.95 ... ∞)	-2.1 (-10 ... 0.27)
RACMO22T/ HadGEM2-ES	1.3 mm/day	1.7 (1.0 ... ∞)	-2.6 (-5.5 ... -0.17)
REMO2009 /EC-EARTH	1.7 mm/day	5.4 (0.36 ... ∞)	-6.6 (-12 ... 5.7)

REMO2009 / HadGEM2-ES	1.7 mm/day	0.84 (0.51 ... ∞)	1.4 (-12 ... 4.0)
REMO2009 / MPI-ESM-LR	1.8 mm/day	0.53 (0.33 ... 59)	2.9 (-7.2 ... 8.1)
REMO2009 /IPSL-CM5A-LR	1.9 mm/day	1.1 (0.80 ... ∞)	-0.50 (-8.2 ... 1.8)
REMO2009 /MIROC5	1.7 mm/day	3.5 (1.3 ... ∞)	-6.6 (-12 ... -1.6)
HadGEM3-GC31-HM HighresMIP	1.6 mm/day	3.8 (0.24 ... 23)	-9.3 (-15 ... 4.6)
EC-Earth3P-HR HighresMIP	1.8 mm/day	0.57 (0.00022 ... 2.2e+2)	1.6 (-13 ... 21)
MPI-ESM1-2-XR HighresMIP	1.9 mm/day	0.0084 (0.0018 ... 1.6)	51 (-4.5 ... 84)
GFDL/AM2.5C360	2.6 mm/day	0.19 (0.084 ... 1.8)	8.8 (-3.2 ... 13)
FLOR	1.8 mm/day	1.0 (0.47 ... 4.3)	-0.064 (-6.0 ... 3.3)

Table 4: Analysis results showing the model threshold for a 1-in-135 year event in the current climate, and the probability ratios and intensity changes for the present climate with respect to a pre-industrial climate which is 1.2°C cooler than today. Note that the values listed for ERA5 and CHIRPS in the second column refer to the observed event magnitudes.

The CORDEX models show a modest drying tendency for 24-month low-rainfall extremes, with a small majority of models showing a probability ratio larger than 1. However, few of these models exhibit a significant drying trend, as was the case for the corresponding HiResMIP and GFDL multi-member ensembles.

As a brief sensitivity test, we also considered an alternative definition of the drought index (Figure 12), analysing rainfall accumulations over a 12-month period (still July-June) instead of a 24-month period with the CORDEX-Africa ensemble. Of those 20 CORDEX models included in the 24-month analysis (where seven showed a best-guess PR at or below 1), only two have a corresponding (best-guess) probability ratio below one when looking at 12-month precipitation deficits. However, it is stressed that the majority of these individual models which show a small increase in the likelihood of extreme dryness over twelve months also remain statistically insignificant.

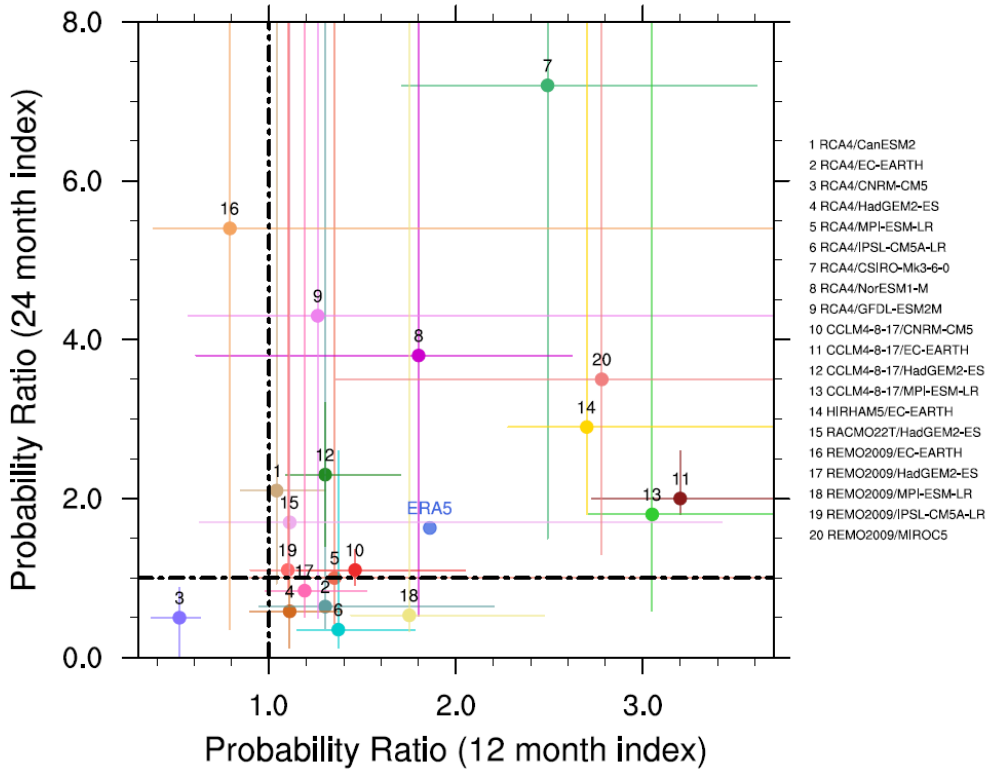

Figure 12: Scatter plot of the Probability Ratio calculated with a 12-month precipitation index, relative to the default Probability Ratio for the 24-month precipitation index. Results are presented for all CORDEX ensemble members (dots with numbers above corresponding to the model used), with their related uncertainties (colored lines) and the ERA5 best-guess probability ratio also shown. Black dashed lines denote a probability ratio of 1.

6. Hazard synthesis

This section shows Probability Ratios and change in intensity (ΔI) for models, while also including the values calculated from the fits with observations. We synthesise the models with the observations to give an overarching attribution statement (please see e.g. Kew et al. (2021) for details on the synthesis technique including how weighting is calculated for observations and for models).

Observations and models are combined into a single result in two ways. First, we neglect common model uncertainties beyond the averaged model spread that is depicted by the bright red bar, and compute the weighted average of models and observations: this is indicated by the magenta bar. The weighting applied is the inverse square of the variability (the width of the bright bars). Second, model uncertainty can be larger than the model spread because of common model uncertainties: we thus also show the more conservative estimate of an unweighted average of observations and models, indicated by the white box accompanying the magenta bar in the synthesis figures.

Figures 13 and 14 show the synthesis results for the current vs. past climate. For the intensity change (that is, the change in total rainfall associated with a 1-in-135 year drought when comparing the past and present climate), we report the weighted synthesis value. Where the results for the probability ratio do not give a finite number we replace them by 10000, to allow all models to be included in the synthesis analysis (sensitivity tests with alternative values yielded no effect on the final results (not shown)). This means that the reported synthesized probability ratio gives a more conservative, lower value.

Results for current vs past climate, or for 1.2°C of global warming vs pre-industrial conditions in 1850-1900, indicate a non-significant change in total rainfall associated with a 24-month drought like the one recently observed, of -2.1% (95% CI: -7.4% to 3.8%). Note that a negative change in intensity means a shift towards drier extremes.

Results also show a non-significant probability ratio of 1.36 (95% CI: 0.50-3.39), with values larger than one indicating a shift towards drier extremes. This means that if a 24-month drought event has a return period of 135 years in the current climate (as is our best estimate for the observed event), then an equivalent event would have a return period of 180 years in a pre-industrial climate, though uncertainty remains high and this latter number could range from as low as 70 years to as high as 450 years.

We conclude that even though models show, on average, a small increase of major 2-year droughts like the 2019-2021 one, the trend is not statistically significant compared to natural variability.

Figure 13: Synthesis of probability ratios, when comparing the 2019-21 event with a pre-industrial climate.

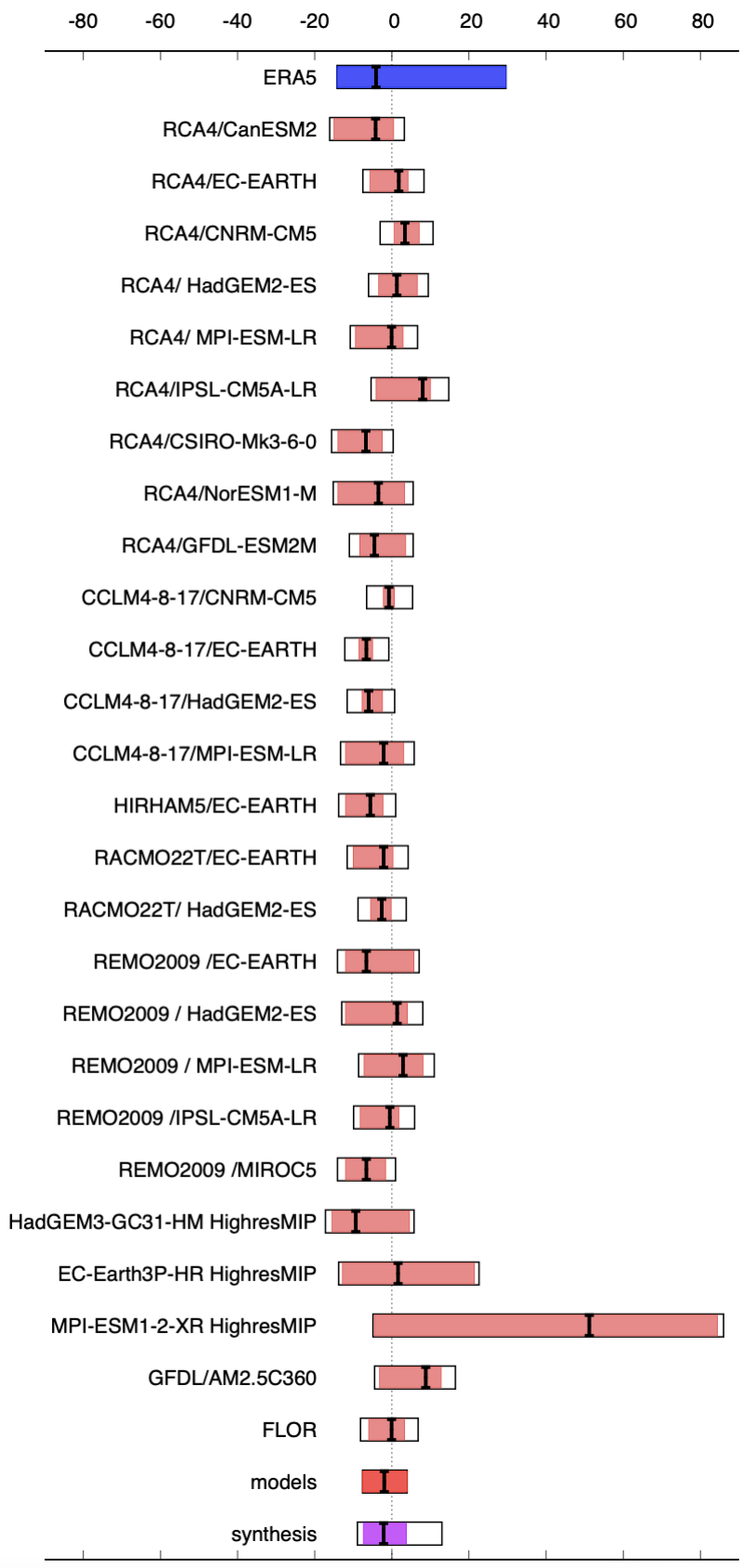

Figure 14: Synthesis figure, showing percent changes in 24-month total rainfall, when comparing the 2019-21 event with an event of an equivalent return period in the pre-industrial climate.

7. Vulnerability and exposure

Food insecurity in Madagascar is not just driven by meteorological drought, but also a host of factors such as demographics, poverty, infrastructure, policy and non-climate shocks and stresses that modify the likelihood of a household becoming food insecure. In this section, we provide an overview of the vulnerability and exposure factors to provide a more nuanced understanding of what is contributing to the ongoing food crisis, and to put our analysis of the climate drivers into context.

Madagascar is amongst the poorest countries in the world, currently ranking 164th out of 189 countries on the human development index[1] (HDI). However, Madagascar's HDI value has seen a steady increase since 1990, showing higher life expectancy and education levels, albeit a decreasing Gross National Income (GNI) per capita despite a relatively stable population growth of 2.6% annually (Human Development Report, 2020; World Bank). Prior to the COVID-19 pandemic, its economy was also growing, notably bolstered by new political stability, and poverty rates were decreasing (World Bank, 2020). Chronic food insecurity and malnutrition is pervasive in Madagascar. In 2020, it was estimated that the country ranked fourth highest in the world in rates of malnutrition, with almost half of the children of 5 years or younger suffering from stunting (World Bank, 2020; World Food Programme, 2021).

Madagascar's greater southern region ("le Grand Sud") is composed of three districts: Atsimo Andrefana, Androy and Anosy. Its climate mainly falls under the Koppen-Geiger zone of BSh, indicating a hot semi-arid climate, characterised by high average temperatures throughout the year and very low and variable precipitation (Beck et al. 2018; see also Figure S1). Drought is considered a chronic issue in this region (Healy, 2018). Le Grand Sud is home to approximately 2.74 million people, around 11% of the country's total population (UNDP, 2021). It is the least developed part of the country, with a poverty incidence of 91% compared to 77% for the rest of the country (World Bank, N.d.). The people living in this region are primarily pastoralists with small scale livestock and cattle, and they undertake subsistence farming growing crops like cassava, maize and sweet potatoes[2]. Water and road infrastructure in le Grand Sud is extremely poor with many roads becoming impassable during the rainy season, cutting off the region from the rest of the country (Healy, 2018). Due to sparsely-distributed and poorly-maintained roads (WFPGeoNode, 2017), road disruptions can easily turn into a paralysis of the whole transport network, in turn slowing down market access and ease of movement, increasing food prices and posing barriers to humanitarian response and food aid distribution. Despite roads being the backbone of intra-country trade, there has been little investment in infrastructure in the last 10 years (The World Bank, 2017, p. 28). In Le Grand Sud, most rivers dry up for part of the year, groundwater is of poor quality and many previously dug boreholes are failing, indicating poor water availability for daily needs (Healy, 2018).

The main rainy season in Madagascar is from November to March, which is a critical period for the majority of farmers that depend on rain-fed agriculture. December to March is the lean season when food tends to run out from last year's harvest, but there is not yet new food from this year's crops. When drought, locusts, storms, pests and a variety of other shocks and stresses result in lower yields, people in this region tend to sell their belongings in order to buy food (Healy, 2018). In southwestern Madagascar, Zebu cattle are herded and hold strong socio-cultural value as well as being an important coping mechanism during drought years. During the 2013-2014 rainy season, one with widespread

[1] http://hdr.undp.org/sites/default/files/Country-Profiles/MDG.pdf
[2] https://fews.net/southern-africa/madagascar/livelihood-zone-map/march-2018

crop failure, people sold their livestock and this accounted for over 56% of cash food expenditures. The second most important income source were remittances from household members who had migrated to other parts of the country for work, and many people (72% of those studied) also received food aid from NGOs (Hänke and Barkmann, 2017).

The 2019-2020 rainy season in southern Madagascar was below normal resulting in crop losses, reduced pasture and drinking water for animals (FEWS NET March 2020). COVID-19 also reached Madagascar in March 2020: the government limited movement to reduce the spread of the virus, but this has inadvertent side effects on incomes and food security discussed later in this section. In its June 2021 update, FEWS NET estimated that "2021 crop production in southern Madagascar is 10-30 percent below last year and 50-70 percent below the five-year average", due to a combination of sandstorms, infestations of both Fall Armyworm and migratory locusts, and low household seedstocks from 2020's high seed prices and low yields (FEWS NET June 2021).

In response to the drought and food insecurity crisis, an emergency plan to address the drought was launched by the Malagasy president at the end of August 2021 (République de Madagascar, 2021). In February 2021, the Malagasy government and UN OCHA made a flash appeal for disaster response for USD 75.9 million to 1.11 million people mainly for food security, nutrition, and WASH initiatives (OCHA 2021). Government and per-government initiatives on the ground since 2021 include the building and maintenance of critical water infrastructure such as the rehabilitation of boreholes, water quality analyses, and food aid and assistance (see above links).

There are also long-term policies and measures in place to reduce the impact of food insecurity in this region. For example, the government has a national drought contingency plan (2013-15) that activates based on the crossing of a threshold of emergency indicators such as comparative rainfall, food prices, water availability, social protection admissions and more (Repoblikan'i Madagasikara, 2012; Razanakoto, 2017). However, the plan focuses on drought and does not address the chronic structural food insecurity and structural vulnerability discussed above. The focus on drought as the main driver of food and nutrition insecurity can also lead to confusion and distort decision-making because, while low rainfall may be a factor, structural vulnerabilities, such as marginalisation, limited livelihood options and poverty, are often more important and need to be addressed to reduce long-term food insecurity (Razanakoto, 2017). In addition, biodiversity conservation policies, cropland expansion, and land privatization have negatively impacted pastoralism as a traditional approach to living in this semi-arid region. Security threats have also resulted in spatial and temporal shifts in grazing patterns which have a compounding impact as well leading to the risk of overgrazing and rangeland degradation (Hänke and Barkmann, 2017).

Madagascar is currently insured under the African Risk Capacity Insurance, with premiums paid in full by the African Development Bank (ARC, 2021). It received its first payout of USD 2.13 million in July 2020 to support anticipated livelihood losses due to crop failure (AfDB, 2020). A drought and food security early warning system (Système d'Alerte Precoce or SAP) was established in 2005 to monitor food security in the Grand Sud, and it has changed administrators a number of times since (IFRC, 2014). Different international agencies are supporting the government with early warnings, including the Food and Agriculture Organisation which publishes a report on food security and agriculture every quarter and ranks risks by their likelihood and potential impact (FAO, 2019). Until last year, UNICEF worked with the Ministère de l'Eau, de l'Hygiène et de l'Assainissement to develop a monitoring system for the South in which bulletins were published every month, reporting

on precipitation and NDVI anomalies based on CHIRPS and MODIS data compared to historical trends (UNICEF, 2020).

In 2015, the country adopted its first National Social Protection Policy (MPPSPF, 2015). Under the national SP policy, the government launched three main cash-transfer programmes: the cash-for work or Productive Safety Net programme, the Human Development Cash Transfer for families with young children, and the FIAVOTA response for drought affected households. According to the World Bank, these main cash-transfer programmes covered 2.5 million people (9% of the total population) between 2019 and 2021. However, certain barriers to the policies effectiveness have been highlighted in the literature, including fragmented cash-transfer programmes, low coverage, a lack of coordination, and low public expenditure to support the programmes (Rabi, 2019). Efforts to increase the coherence of the system are underway (see Berrou et al. 2021). In addition, the World Bank has provided three grants intended to aid in development. The first is a USD 90 million grant (approved in March 2019) to support the social safety programme; the second a USD 100 million IDA grant (approved in December 2020) to "improve access to basic infrastructure and livelihood opportunities and strengthen local governance in southern Madagascar", and the third a grant of USD 150 million (approved in March 2021) for the country's social safety programme including the COVID-19 social protection response (World Bank, 2021).

The COVID-19 pandemic was an important risk multiplier in the food insecurity crisis, a dynamic that has played out in a multitude of countries around the world (IFRC 2021). During March of 2020 the first COVID cases were reported in Madagascar's capital city, Antananarivo, and the government enacted measures to reduce spread, including limiting public transport and short-term lockdowns (FEWS NET March 2020). The measures dramatically "reduced income-earning opportunities among daily wage laborers and led to a large-scale urban exodus", in which people chose to return to homes in rural areas and resume agriculture activities and earn a reduced income (FEWS NET April 2020, May 2020). Wages for agricultural laborers declined as more people were looking for jobs locally following the exodus, and migration further afield became more difficult (Ibid.). Sanitary checks at ports also increased the price of imported goods: this affected the poorest populations most as they rely on imported rice, for example, during below-average harvest years (FEWS NET May 2020). Even after most restrictions were lifted, the laborers could not migrate to western and northern parts of the country as they usually would, because the only roads to get there go through the cities that remained under lockdown (FEWS NET June 2020). And in many places, restrictions were then reinstated by July 2020 when COVID-19 cases skyrocketed in the country (FEWS NET July 2020).

Overall, the stay-at-home orders and other measures, necessary to limit the spread of COVID-19 and prevent health infrastructure from being overwhelmed, negatively impacted people's ability to migrate for casual labor – a key source of income for people and communities in Southern Madagascar to modulate the negative impacts of a poor yield year. (FEWS NET April 2020, FEWS NET June 2021) The COVID-19 measures disrupted supply chains around the world and within Madagascar, exacerbating price hikes for staple foods and limiting access to markets (FEWS NET April 2020). The tourism, mining and textile industries were also disrupted by COVID-19, which in turn reduced the number of jobs available for those who were able to migrate once restrictions were lifted, thereby having a dampening effect on the local economy (FEWS NET Oct 2020, FEWSNET Sep 2021). This lack of alternative income sources led to more people reliant on farming to make a living.

Finally, in its September 2021 update on the food security situation in Southern Madagascar, FEWS NET projects that despite likely rainfall near average in the October 2021 to May 2022 range, the southern regions food insecurity will likely persist due to insufficient seed and cutting supplies from previous poor productivity seasons, average pest attacks, with "near zero" capacity for pest control, and continued below normal casual labor opportunities due to continued effects of the COVID-19 pandemic (FEWS NET Sep 2021). This combination of factors underscores the complexity of regional food security in general as well as the difficulty to 'bounce back' following failed seasons even if a rainy season is climatologically normal.

The semi-arid climate of le Grand Sud is a challenging backdrop for subsistence farming, even in meteorologically "normal" years. Vulnerability in this region is high due to the interplay of poverty, structural underinvestments in development, especially historically, and land use policies that have diminished pastoralist options, among other factors. This backdrop has combined with a series of reduced rainfall years and the limitations posed by the COVID-19 pandemic, making a challenging situation worse. While climate change did not play a statistically significant role in the reduced rainfall that contributed to this current food crisis, as noted in other parts of this paper, the impacts currently being felt by the combination of hazard, vulnerability and exposure in this region are a warning sign for the future. This also points to an opportunity to avert future harm: structural investments, such as those that are currently underway, have the potential to improve critical infrastructure, strengthen social protection systems and diversify livelihood opportunities. Investments such as these will become even more crucial if global warming continues at current rates. For example, should global warming exceed 2°C, there is *medium confidence* that agricultural and agro-ecological droughts may increase in Madagascar as a whole (IPCC AR6 2021). This could further increase risks of food insecurity, if the vulnerability of people and systems are not reduced.

Data availability

Data will be made available via the Climate Explorer in the coming days.

Appendix 1 - Comparison of Köppen-Geiger classifications for different regions in Africa

Figure S1, below, shows the diversity of Köppen-Geiger climate zones, based on data from Beck *et al.* (2018). We further highlight similarities in classifications between some of the sub-regions studied in Kew *et al.* (2021; black rectangles), and the region of interest in this study (purple rectangle).

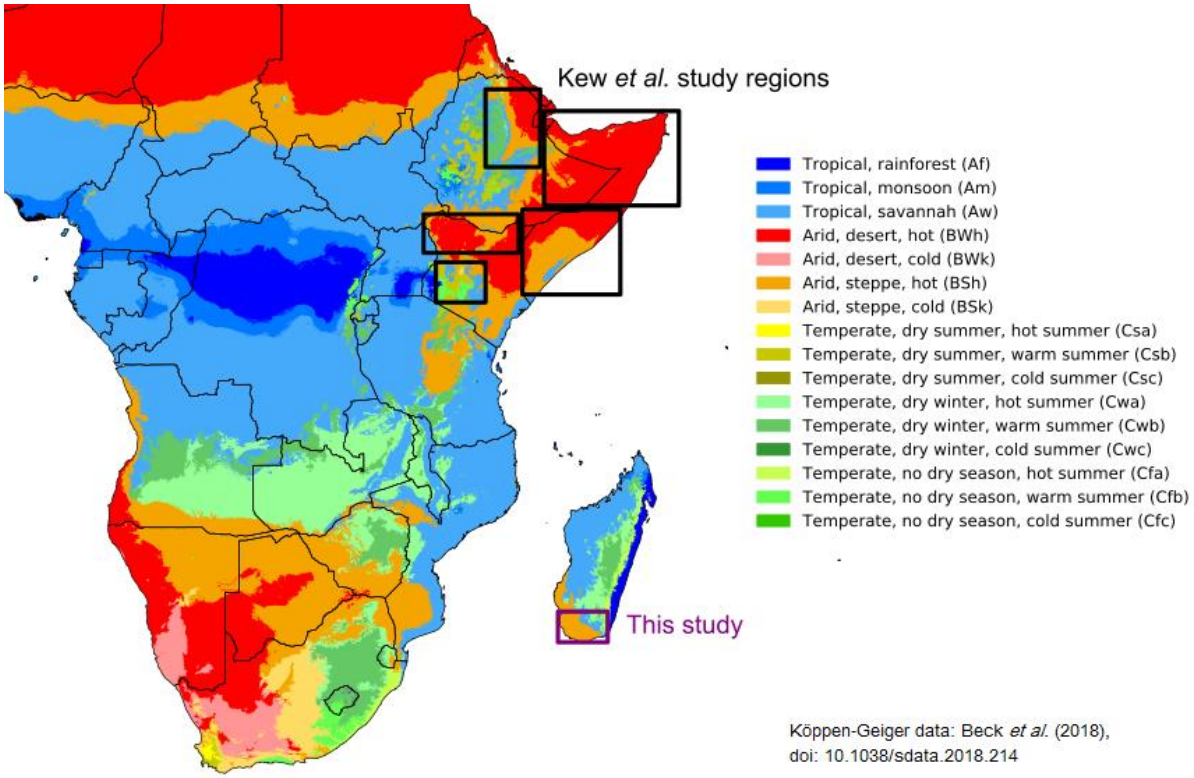

Figure S1: Köppen-Geiger climate classifications across Madagascar and continental Africa (source: Beck et al. 2018, https://doi.org/10.1038/sdata.2018.214). We note the similarity between the Köppen-Geiger zones found in several of the sub-regions studied in Kew *et al.* (2021) and the region of focus for this analysis (purple rectangle).

Appendix 2 - Evaluation of station observations from GHCN-CAMS and TAHMO

TAHMO

We examined available station observations from the Trans-African Hydro-Meteorological Observatory (TAHMO) dataset (https://tahmo.org/climate-data/). Unfortunately, no data was suitable: while one station was identified in the southern part of the country, this was on the eastern coast where climatological rainfall is much larger than in the south-west region of interest. In addition, only five years of data were available for that station.

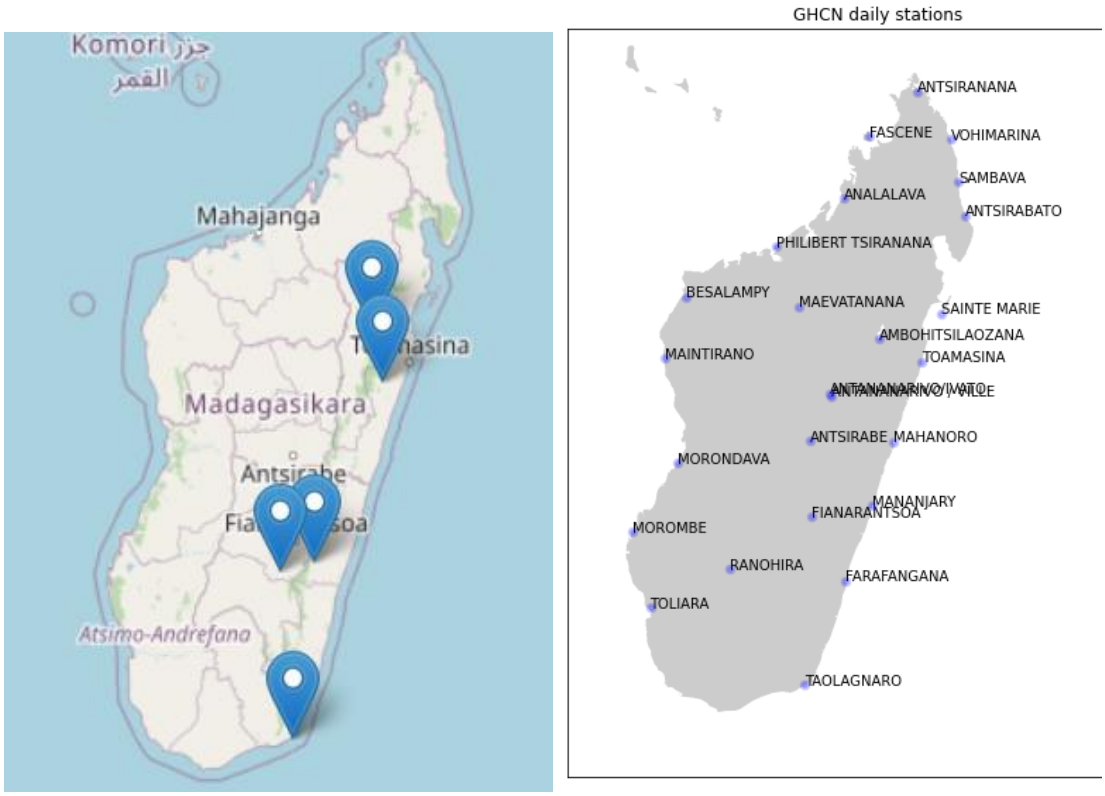

Figure S2: The locations of available weather station data from TAHMO (left) and GHCN-D (right).

GHCN

We extracted daily rainfall data from all available stations in the Global Historical Climatology Network (GHCN) database (available via https://bit.ly/3r6iiUi).

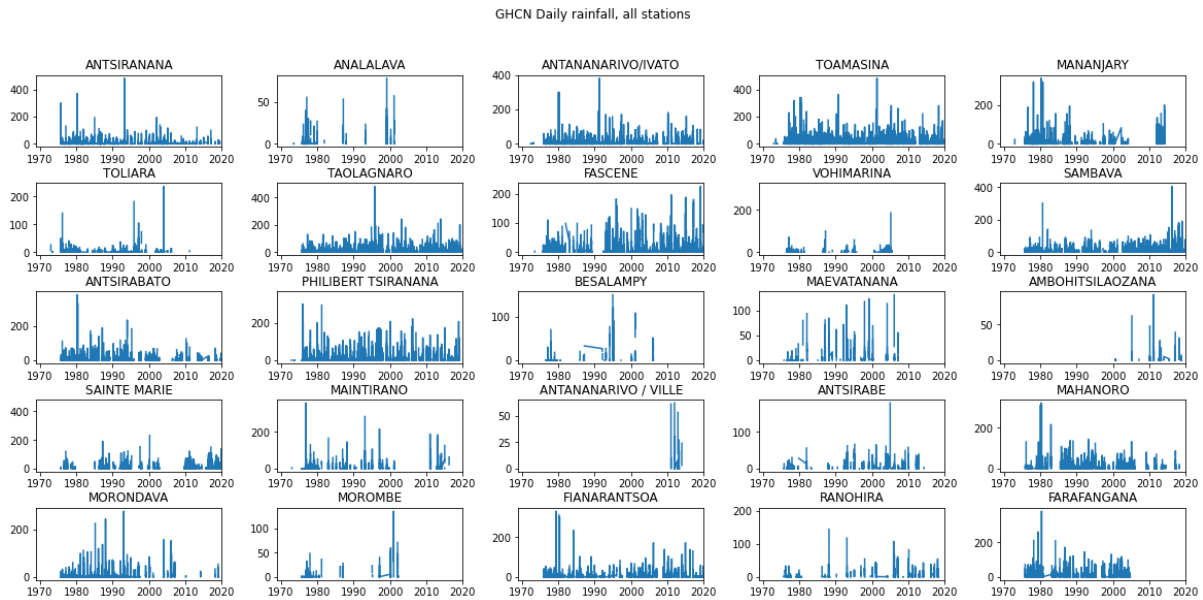

Figure S3: Time series of GHCN-D data (presented as monthly rainfall accumulations, in mm) for all stations.

When focusing on those stations which were located in the southern region of Madagascar of interest, only four stations were relevant (see below). After further accounting for missing data within their respective time-series, only the station from Taolagnaro appeared suitable for analysis.

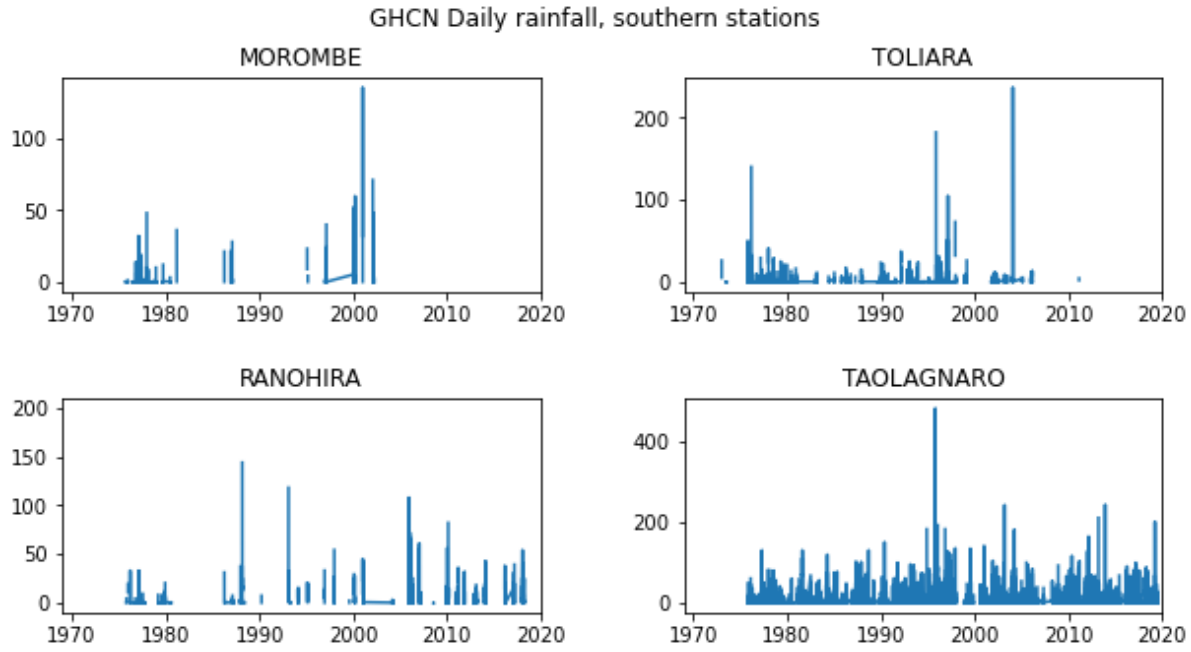

Figure S4: Time series of available GHCN-D data (presented as monthly rainfall accumulations, in mm) for all southern stations.

However, when interrogating further (see below), we found this station to also have "missing data" days recorded frequently (marked as NA in the data). Moreover, this pattern changed in time - there was an increase in no-data days around 2010, and an associated reduction in dry days (days with rainfall==0). Such behaviour was present in DJF rainfall too, and we therefore concluded it was not a defensible source of data to use for further analysis.

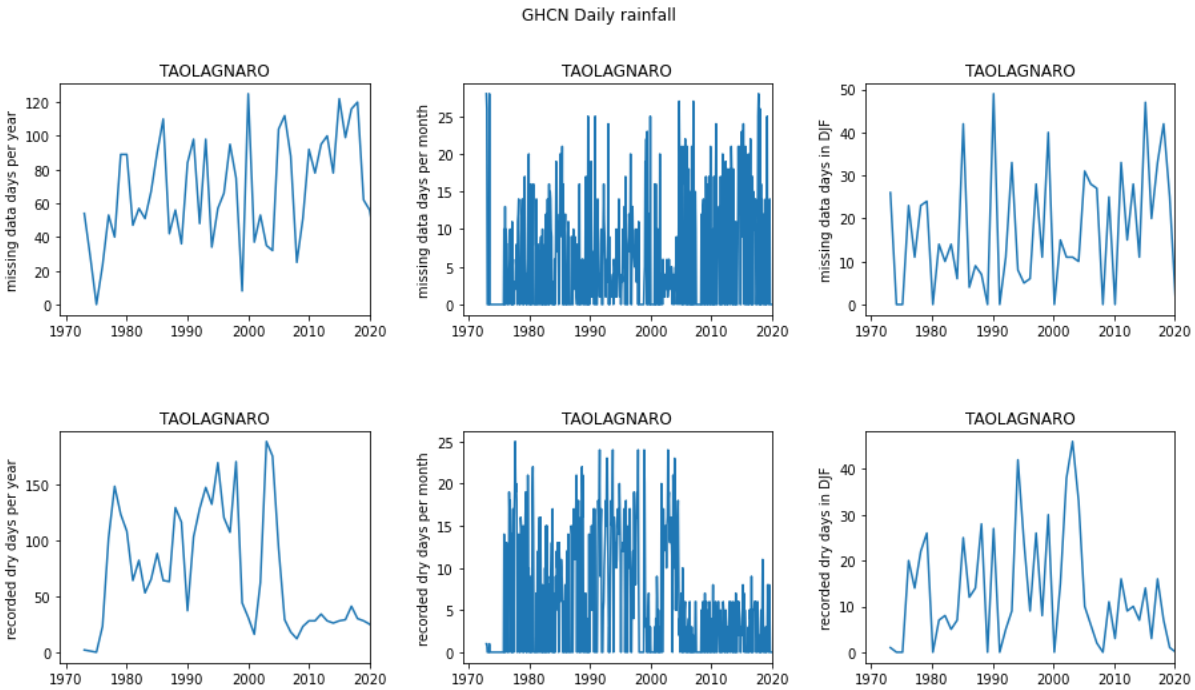

Figure S5: Time series of "missing data" days (top row) and "dry days" (bottom row) for Taolagnaro station. The left-hand columns show number of days falling under each category per year; the middle columns show the values for each month; the right-hand columns show the number of days falling under each category summed across the months of DJF for each year.

References

Abram, N. J., Wright, N. M., Ellis, B., Dixon, B. C., Wurtzel, J. B., England, M. H., et al. (2020). Coupling of Indo-Pacific climate variability over the last millennium. *Nature*, *579*(7799), 385–392. https://doi.org/10.1038/s41586-020-2084-4

Barimalala, R., Raholijao, N., Pokam, W., & Reason, C. J. C. (2021). Potential impacts of 1.5 °C, 2 °C global warming levels on temperature and rainfall over Madagascar. *Environmental Research Letters*, *16*(4), 044019. https://doi.org/10.1088/1748-9326/abeb34

Barimalala, R., Desbiolles, F., Blamey, R. C., & Reason, C. (2018). Madagascar Influence on the South Indian Ocean Convergence Zone, the Mozambique Channel Trough and Southern African Rainfall. *Geophysical Research Letters*, *45* (20), 11,380-11,389. https://doi.org/10.1029/2018GL079964

Beck, H. E., Zimmermann, N. E., McVicar, T. R., Vergopolan, N., Berg, A., & Wood, E. F. (2018). Present and future Köppen-Geiger climate classification maps at 1-km resolution. *Scientific Data*, *5*(1), 180214. https://doi.org/10.1038/sdata.2018.214

Benson, C. & Clay, E. (1998). *The Impact of Drought on Sub-Saharan African Economies* (The World Bank).

Berrou, J.-P., Piveteau, A., Deguilhem, T., Delpy, L., & Gondard-Delcroix, C. (2021). *Who Drives if No-one Governs? A Social Network Analysis of Social Protection Policy in Madagascar* (SSRN Scholarly Paper No. ID 3811178). Rochester, NY: Social Science Research Network. Retrieved from https://papers.ssrn.com/abstract=3811178

Cai, W., Yang, K., Wu, L., Huang, G., Santoso, A., Ng, B., et al. (2021). Opposite response of strong and moderate positive Indian Ocean Dipole to global warming. *Nature Climate Change*, *11*(1), 27–32. https://doi.org/10.1038/s41558-020-00943-1

Chan, D., Vecchi, G., Yang, W., and Huybers, P.: Improved simulation of 19th-and 20th-century North Atlantic hurricane frequency after correcting historical sea surface temperatures, *Science Advances*, 7, https://doi.org/10.1126/sciadv.abg6931

Ciavarella, A., Cotterill, D., Stott, P., Kew, S., Philip, S., van Oldenborgh, G. J., et al. (2021). Prolonged Siberian heat of 2020 almost impossible without human influence. *Climatic Change*, *166* (1), 9. https://doi.org/10.1007/s10584-021-03052-w

Coppola, E., Raffaele, F., Giorgi, F., Giuliani, G., Xuejie, G., Ciarlo, J. M., et al. (2021). Climate hazard indices projections based on CORDEX-CORE, CMIP5 and CMIP6 ensemble. *Climate Dynamics*, *57*(5), 1293–1383. https://doi.org/10.1007/s00382-021-05640-z

Dosio, A., Jones, R. G., Jack, C., Lennard, C., Nikulin, G., & Hewitson, B. (2019). What can we know about future precipitation in Africa? Robustness, significance and added value of projections from a large ensemble of regional climate models. *Climate Dynamics*, *53*(9), 5833–5858. https://doi.org/10.1007/s00382-019-04900-3

FAO (2015). *The impact of disasters on agriculture and food security*. 1-54. https://www.fao.org/publications/card/en/c/fa17f187-9b92-439f-9952-1d6c13d14782/

Fauchereau, N., Pohl, B., Reason, C. J. C., Rouault, M., & Richard, Y. (2009). Recurrent daily OLR patterns in the Southern Africa/Southwest Indian Ocean region, implications for South African rainfall and teleconnections. *Climate Dynamics*, *32*(4), 575–591. https://doi.org/10.1007/s00382-008-0426-2

Favre, A., Hewitson, B., Lennard, C., Cerezo-Mota, R., & Tadross, M. (2013). Cut-off Lows in the South Africa region and their contribution to precipitation. *Climate Dynamics*, *41*(9), 2331–2351. https://doi.org/10.1007/s00382-012-1579-6

FEWS NET March 2020. https://fews.net/southern-africa/madagascar/key-message-update/march-2020

FEWS NET April 2020. https://fews.net/southern-africa/madagascar/food-security-outlook-update/april-2020

FEWS NET May 2020. https://fews.net/southern-africa/madagascar/key-message-update/may-2020

FEWS NET June 2020. https://fews.net/sites/default/files/documents/reports/MADAGASCAR_Food_Security_Outlook_June2020_Final_EN.pdf

FEWS NET July 2020. https://fews.net/southern-africa/madagascar/key-message-update/july-2020

FEWS NET October 2020. https://fews.net/sites/default/files/documents/reports/Madagascar_Outlook_Oct2020_Final_EN_1.pdf

FEWS NET June 2021. https://fews.net/southern-africa/madagascar/alert/june-10-2021

FEWS NET September 2021. https://fews.net/southern-africa/madagascar

Funk, C., Peterson, P., Landsfeld, M., Pedreros, D., Verdin, J., Shukla, S., et al. (2015). The climate hazards infrared precipitation with stations—a new environmental record for monitoring extremes. *Scientific Data*, *2*(1), 150066. https://doi.org/10.1038/sdata.2015.66

Haarsma, R. J., Roberts, M. J., Vidale, P. L., Senior, C. A., Bellucci, A., Bao, Q., et al. (2016). High Resolution Model Intercomparison Project (HighResMIP v1.0) for CMIP6. *Geoscientific Model Development*, *9*(11), 4185–4208. https://doi.org/10.5194/gmd-9-4185-2016

Hänke, H., & Barkmann, J. (2017). Insurance function of livestock, Farmers coping capacity with crop failure in southwestern Madagascar. *World Development*, *96*, 264–275. https://doi.org/10.1016/j.worlddev.2017.03.011

Hansen, J., Ruedy, R., Sato, M., & Lo, K. (2010). Global Surface Temperature Change. *Reviews of Geophysics*, *48*(4). https://doi.org/10.1029/2010RG000345

Hart, N. C. G., Reason, C. J. C., & Fauchereau, N. (2013). Cloud bands over southern Africa: seasonality, contribution to rainfall variability and modulation by the MJO. *Climate Dynamics*, *41*(5), 1199–1212. https://doi.org/10.1007/s00382-012-1589-4

Hart, N. C. G., Washington, R., & Reason, C. J. C. (2018). On the Likelihood of Tropical–Extratropical Cloud Bands in the South Indian Convergence Zone during ENSO Events. *Journal of Climate*, *31*(7), 2797–2817. https://doi.org/10.1175/JCLI-D-17-0221.1

Healy et al. (2018). THE DEEP SOUTH, https://bit.ly/3oWVR1d.

Hersbach, H., Bell, B., Berrisford, P., Hirahara, S., Horányi, A., Muñoz-Sabater, J., et al. (2020). The ERA5 global reanalysis. *Quarterly Journal of the Royal Meteorological Society*, *146*(730), 1999–2049. https://doi.org/10.1002/qj.3803

Hoell, A., Funk, C., Magadzire, T., Zinke, J., & Husak, G. (2015). El Niño–Southern Oscillation diversity and Southern Africa teleconnections during Austral Summer. *Climate Dynamics*, *45*(5), 1583–1599. https://doi.org/10.1007/s00382-014-2414-z

Hoell, A., Funk, C., Zinke, J., & Harrison, L. (2017). Modulation of the Southern Africa precipitation response to the El Niño Southern Oscillation by the subtropical Indian Ocean Dipole. *Climate Dynamics*, *48*(7), 2529–2540. https://doi.org/10.1007/s00382-016-3220-6

IFRC (2021). The compound impact of extreme weather events and COVID-19. https://www.ifrc.org/media/49590

IPC (2021). Madagascar: Acute Food Insecurity and Acute Malnutrition Situation April 2021 - April 2022. https://bit.ly/3kQsKeT

IPCC, 2021: *Climate Change 2021: The Physical Science Basis. Contribution of Working Group I to the Sixth Assessment Report of the Intergovernmental Panel on Climate Change* [Masson-Delmotte, V., P. Zhai, A. Pirani, S.L. Connors, C. Péan, S. Berger, N. Caud, Y. Chen, L. Goldfarb, M.I. Gomis, M. Huang, K. Leitzell, E. Lonnoy, J.B.R. Matthews, T.K. Maycock, T. Waterfield, O. Yelekçi, R. Yu, and B. Zhou (eds.)]. Cambridge University Press. In Press.

Jury, M. R., Parker, B. A., Raholijao, N., & Nassor, A. (1995). Variability of summer rainfall over Madagascar: Climatic determinants at interannual scales. *International Journal of Climatology*, *15*(12), 1323–1332. https://doi.org/10.1002/joc.3370151203

Jury, M. R. (2016). Summer climate of Madagascar and monsoon pulsing of its vortex. *Meteorology and Atmospheric Physics*, *128*(1), 117–129. https://doi.org/10.1007/s00703-015-0401-5

Kendon, E. J., Stratton, R. A., Tucker, S., Marsham, J. H., Berthou, S., Rowell, D. P., & Senior, C. A. (2019). Enhanced future changes in wet and dry extremes over Africa at convection-permitting scale. *Nature Communications*, *10*(1), 1794. https://doi.org/10.1038/s41467-019-09776-9

Kew, S. F., Philip, S. Y., Hauser, M., Hobbins, M., Wanders, N., van Oldenborgh, G. J., et al. (2021). Impact of precipitation and increasing temperatures on drought trends in eastern Africa. *Earth System Dynamics*, *12*(1), 17–35. https://doi.org/10.5194/esd-12-17-2021

Klinman, M. G., & Reason, C. J. C. (2008). On the peculiar storm track of TC Favio during the 2006–2007 Southwest Indian Ocean tropical cyclone season and relationships to ENSO. *Meteorology and Atmospheric Physics*, *100*(1), 233–242. https://doi.org/10.1007/s00703-008-0306-7

Lenssen, N. J. L., Schmidt, G. A., Hansen, J. E., Menne, M. J., Persin, A., Ruedy, R., & Zyss, D. (2019). Improvements in the GISTEMP Uncertainty Model. *Journal of Geophysical Research: Atmospheres*, *124*(12), 6307–6326. https://doi.org/10.1029/2018JD029522

Lim Kam Sian, K. T. C., Wang, J., Ayugi, B. O., Nooni, I. K., & Ongoma, V. (2021). Multi-Decadal Variability and Future Changes in Precipitation over Southern Africa. *Atmosphere*, *12*(6), 742. https://doi.org/10.3390/atmos12060742

Macron, C., Richard, Y., Garot, T., Bessafi, M., Pohl, B., Ratiarison, A., & Razafindrabe, A. (2016). Intraseasonal Rainfall Variability over Madagascar. *Monthly Weather Review*, *144*(5), 1877–1885. https://doi.org/10.1175/MWR-D-15-0077.1

Manning, C., Widmann, M., Bevacqua, E., Loon, A. F. V., Maraun, D., & Vrac, M. (2018). Soil Moisture Drought in Europe: A Compound Event of Precipitation and Potential Evapotranspiration on Multiple Time Scales. *Journal of Hydrometeorology*, *19*(8), 1255–1271. https://doi.org/10.1175/JHM-D-18-0017.1

Nikulin, G., Jones, C., Giorgi, F., Asrar, G., Büchner, M., Cerezo-Mota, R., et al. (2012). Precipitation Climatology in an Ensemble of CORDEX-Africa Regional Climate Simulations. *Journal of Climate*, *25*(18), 6057–6078. https://doi.org/10.1175/JCLI-D-11-00375.1

Padrón, R. S., Gudmundsson, L., Decharme, B., Ducharne, A., Lawrence, D. M., Mao, J., et al. (2020). Observed changes in dry-season water availability attributed to human-induced climate change. *Nature Geoscience*, *13*(7), 477–481. https://doi.org/10.1038/s41561-020-0594-1

Philip, S., Kew, S., van Oldenborgh, G. J., Otto, F., Vautard, R., van der Wiel, K., et al. (2020). A protocol for probabilistic extreme event attribution analyses. *Advances in Statistical Climatology, Meteorology and Oceanography*, *6*(2), 177–203. https://doi.org/10.5194/ascmo-6-177-2020

Ranasinghe, R., A.C. Ruane, R. Vautard, N. Arnell, E. Coppola, F.A. Cruz, S. Dessai, A.S. Islam, M. Rahimi, D. Ruiz Carrascal, J. Sillmann, M.B. Sylla, C. Tebaldi, W. Wang, and R. Zaaboul, 2021: Climate Change Information for Regional Impact and for Risk Assessment. In *Climate Change 2021: The Physical Science Basis. Contribution of Working Group I to the Sixth Assessment Report of the Intergovernmental Panel on Climate Change* [MassonDelmotte, V., P. Zhai, A. Pirani, S.L. Connors, C. Péan, S. Berger, N. Caud, Y. Chen, L. Goldfarb, M.I. Gomis, M. Huang, K. Leitzell, E. Lonnoy, J.B.R. Matthews, T.K. Maycock, T. Waterfield, O. Yelekçi, R. Yu, and B. Zhou (eds.)]. Cambridge University Press. In Press.

Randriamahefasoa, T. S. M., & Reason, C. J. C. (2017). Interannual variability of rainfall characteristics over southwestern Madagascar. *Theoretical and Applied Climatology*, *128*(1), 421–437. https://doi.org/10.1007/s00704-015-1719-0

Randriamarolaza, L. Y. A., Aguilar, E., Skrynyk, O., Vicente-Serrano, S. M., & Domínguez-Castro, F. (2021). Indices for daily temperature and precipitation in Madagascar, based on quality-controlled and homogenized data, 1950–2018. *International Journal of Climatology*, *n/a*(n/a). https://doi.org/10.1002/joc.7243

N. A. Rayner, D. E. Parker, E. B. Horton, C. K. Folland, L. V. Alexander, D. P. Rowell, E. C. Kent, A. Kaplan, Global analyses of sea surface temperature, sea ice, and night marine air temperature since the late nineteenth century. J. Geophys. Res. Atmos. 108, D14 (2003).

Razanakoto, T. (2017) *Analyse de la vulnerabilite a la secheresse des familles paysannes Tandroy* [Unpublished doctoral thesis] University of Antananarivo.

Reason, C. J. C. (2007). Tropical cyclone Dera, the unusual 2000/01 tropical cyclone season in the South West Indian Ocean and associated rainfall anomalies over Southern Africa. *Meteorology and Atmospheric Physics*, *97*(1), 181–188. https://doi.org/10.1007/s00703-006-0251-2

Seneviratne, S.I., X. Zhang, M. Adnan, W. Badi, C. Dereczynski, A. Di Luca, S. Ghosh, I. Iskandar, J. Kossin, S. Lewis, F. Otto, I. Pinto, M. Satoh, S.M. Vicente-Serrano, M. Wehner, and B. Zhou, 2021: Weather and Climate Extreme Events in a Changing Climate. *In Climate Change 2021: The Physical Science Basis. Contribution of Working Group I to the Sixth Assessment Report of the Intergovernmental Panel on Climate Change* [MassonDelmotte, V., P. Zhai, A. Pirani, S.L. Connors, C. Péan, S. Berger, N. Caud, Y. Chen, L. Goldfarb, M.I. Gomis, M. Huang, K. Leitzell, E. Lonnoy, J.B.R. Matthews, T.K. Maycock, T. Waterfield, O. Yelekçi, R. Yu, and B. Zhou (eds.)]. Cambridge University Press. In Press.

Taylor, K. E., Stouffer, R. J., & Meehl, G. A. (2012). An Overview of CMIP5 and the Experiment Design. *Bulletin of the American Meteorological Society*, *93*(4), 485–498. https://doi.org/10.1175/BAMS-D-11-00094.1

van Loon, A. F., Gleeson, T., Clark, J., Van Dijk, A. I. J. M., Stahl, K., Hannaford, J., et al. (2016). Drought in the Anthropocene. *Nature Geoscience*, *9*(2), 89–91. https://doi.org/10.1038/ngeo2646

van Oldenborgh, G. J., van der Wiel, K., Kew, S., Philip, S., Otto, F., Vautard, R., et al. (2021). Pathways and pitfalls in extreme event attribution. *Climatic Change*, *166* (1), 13. https://doi.org/10.1007/s10584-021-03071-7

Vecchi, G. A., Delworth, T., Gudgel, R., Kapnick, S., Rosati, A., Wittenberg, A. T., Zeng, F., Anderson, W., Balaji, V., Dixon, K., et al.: On the seasonal forecasting of regional tropical cyclone activity, J. Climate, 27, 7994–8016, https://doi.org/10.1175/JCLI-D-14-00158.1, 2014

Yang, W., Hsieh, T.-L., and Vecchi, G. A.: Hurricane annual cycle controlled by both seeds and genesis probability, Proceedings of the National Academy of Sciences, 118, https://doi.org/10.1073/pnas.2108397118, 2021.